KTH ROYAL INSTITUTE
OF TECHNOLOGY

Doctoral Thesis in Resources, Energy and Infrastructure

Multi-Scale Surface Water-Groundwater Interaction: Implications for Groundwater Discharge Patterns

BRIAN BABAK MOJARRAD

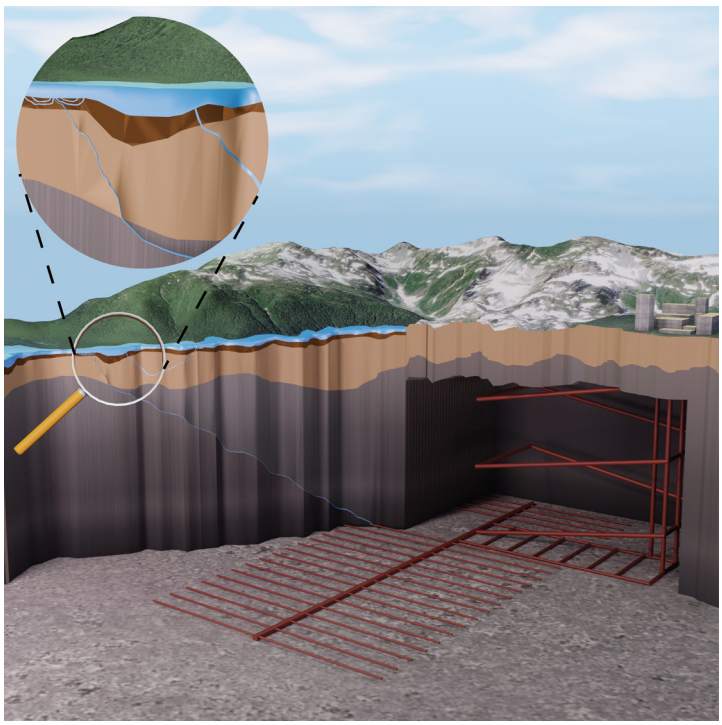

Stockholm, Sweden 2021

Multi-Scale Surface Water-Groundwater Interaction: Implications for Groundwater Discharge Patterns

BRIAN BABAK MOJARRAD

Academic Dissertation which, with due permission of the KTH Royal Institute of Technology, is submitted for public defence for the Degree of Doctor of Philosophy on Friday the 26th November 2021, at 1:00 p.m. in F3, Lindstedsvägen 26, Stockholm.

Doctoral Thesis in Resources, Energy and Infrastructure
KTH Royal Institute of Technology
Stockholm, Sweden 2021

ISBN 978-91-8040-025-1
TRITA-ABE-DLT-2138

Printed by: Universitetsservice US-AB, Sweden 2021

It was the best of times,
It was the worst of times,
It was the age of wisdom,
It was the age of foolishness, …

Charled Dickens

PREFACE

This PhD thesis cosists of summarizing text on applied numerical modelling, applying exact solutions and field investigations leading to the following publications:

Paper I **Mojarrad, B. B.**, Riml, J., Wörman, A., & Laudon, H. (2019). Fragmentation of the hyporheic zone due to regional groundwater circulation. *Water resources research*, *55*(2), 1242-1262.

Paper II **Mojarrad, B. B.**, Betterle, A., Singh, T., Olid, C., & Wörman, A. (2019). The effect of stream discharge on hyporheic exchange. *Water*, *11*(7), 1436.

Paper III Wörman, A., Riml, J., **Mojarrad, B. B.**, & Xu, S. (2019). Parameterizing water fluxes in the geosphere-biosphere interface zone: For use in biosphere modelling as part of the long-term safety assessment. In *17th International High-Level Radioactive Waste Management Conference, IHLRWM 2019, 14-18 April 2019, Knoxville, United States* (pp. 554-558). American Nuclear Society.

Paper IV **Mojarrad, B. B.**, Wörman, A., Riml, J., & Xu, S. (2021). Convergence of groundwater discharge through the hyporheic zone of streams. Submitted.

Paper V Morén, I., **Mojarrad**, **B. B.**, Riml, J., Wörman, A. (2021). Geographic and hydromorphologic controls on surface water–groundwater interactions averaged at different spatial scales, (*Draft manuscript*).

Note that the contribution of the author in each paper are as follows:

Paper I. Responsible for conceptualization, scientific planning, data processing, numerical modelling, exact solution and statistical analysis, writing

Paper II. Responsible for conceptualization, scientific planning, field investigation, data processing, numerical modelling, writing

Paper III. Responsible for scientific planning, data processing, numerical modelling, exact solution analysis

Paper IV. Responsible for conceptualization, scientific planning, data processing, numerical modelling, exact solution and statistical analysis, writing

Paper V. Responsible for scientific planning, data processing, numerical modelling, part of the writing

SUMMARY IN SWEDISH

Vattendrag och akviferer utbyter vatten på olika tids- och längdskalor på grund av bottenformationer och det omgivande landskapets topografi. Samspelet av flöden på olika skalor sker i de permeabla sedimenten under det strömmande ytvatten, i den så kallade hyporheiska zonen. Den hyporheiska zonen är en viktig ekoton där vatten, energi och lösta ämnen som kommer från grundvatten och strömmande ytvatten blandas. Flödet i den hyporheiska zonen är uppdelat på flödesceller i ett hierkiskt storlekssystem (spektrum) av olika storlekar som omfattar från flodbäddens formationer till det regionala landskapets topografi. Det innebär att vattendragets hyporeiska zon påverkar det storskaliga grundvattnets utströmning och tvärtom att grundvattnets utströmning påverkar den hyporeiska zonen. Således måste matematiska analyser av vattenströmningen täcka hela det breda intervallet av skalor för att uppnå en tillräcklig förståelse av det hyporheiska utbytesprocesser. I denna avhandling gjorde jag en uppdelning av det regionala grundvattenflödet och det hyporheiskt flödet och undersökte deras respektive roller för strömningsinteraktionen i vattendragens sediment, samt bedömde vikten av regionala och lokala parametrar för att generalisera ytvatten- och grundvatteninteraktionen. En särskilt viktig fråga var att dela upp randvillkoret för grundvattenytan på de två skalintervallen och samtidigt ta hänsyn till infiltrationens begränsning för grundvattenytan. Det regionala grundvattenflödet utvärderades med hjälp av numerisk modellering med hänsyn till platsspecifik landskapsmorfologi, geologisk heterogenitet i ett svenskt borealt avrinningsområde och hydrologisk information, som infiltration och vattendrasnätverket. En exakt spektral lösning applicerades på det hyporeiska flödet med hänsyn till vattendragets lokala topografi på skalor som inte förekom i den regionala grundvattenanalysen. Graden av osäkerhet i det hydrostatiska och dynamiska bidragen till det hyporheiska flödet undersöktes genom en kombinatorisk indata av bottentopografi och den s.k. ”damping factor” som beskriver ytans form i förhållande till bottens form (Monte Carlo-simulering). Effekterna av det regionala grundvattenflödet på det hierkiska flödessystemet i den hyporeiska zonen studerades genom att superponera flödesfälten. Superponeringen blir ett effektivt tillvägagångssätt för att analysera flödessystemens interaktion eftersom de två skalintervallen kan utvärderas separat. Den hyporheiska flödeshastigheten befanns i normalfallet vara minst en storleksordning högre än grundvattenflödeshastigheten. Detta återspeglar att det hyporheiska flödet dominerar över grundvattenutströmning i bottensedimenten och ger en betydande inverkan på grundvattenflödets residenstid genom den hyporeiska zonen, riktning och det djupa grundvattnets utströmning genom bottensedimentet. Det utströmmande grundvattnet uppvisade en markant “kontraktion” eller ”konvergens” på grund av det hyporeiska flödet och utströmningsområdena begränsades till fragmenterade, små områden som är fördelade längs botten. Resultaten indikerade att både intensiteten på grundvattenflödet i förhållande till grundvattenutströmningen och heterogeniteten hos sedimentet kontrollerade hur djupt det hyporheiska flödet nådde. Dessutom ledde den ökade flödesintensiteten till ett bredare spektrum av hyporeiska flödestransporttider. I ett fältförsök användes

temperaturmätningar för att utvärdera utbredningen av utströmningsområden. Vidare så undersöktes effekterna av en plötslig vattenståndsökning på det hyporheiska flödet med hjälp av en fältstudie där en dammlucka öppnades plötsligt och skapade en flodvåg.

ACKNOWLEDGEMENTS

I gratefully acknowledge the financial support I received from the Swedish Radiation Safety Authority, SSM, (grant agreement No. SSM2015-1753 & SSM2019-1195) and the Marie Curie ITN HypoTRAIN project (which received funding from the European Union's Horizon 2020 research and innovation program under Marie Skłodowska-Curie (grant agreement No. 641939). I would like to thank Maria Nordén and Shulan Xu for providing the financial basis and moral and intellectual support for two SSM projects. Furthermore, I am thankful to Michael Radke for initiating the HypoTRAIN project.

I would like to acknowledge my main supervisor, Anders Wörman, and my co-supervisor, Joakim Riml. Anders, thanks for giving me this life-changing opportunity, for our inspirational dialogues, and for helping me to become a better researcher with your invaluable advice, guidance, and support. I am grateful to Joakim Riml for our many discussions and his selfless assistance in my research. Thanks, Joakim, for always being available.

I would like to express my gratitude to Fulvio Boano (Polytechnic University of Turin) for the arrangement we established and his support during my stay in Turin. Fulvio, thank you for broadening my scientific research horizon and helping me to establish a research network in Italy.

I would like to thank my colleagues and former colleagues at KTH, Polytechnic University of Turin, Elburs football club, and my HypoTRAIN family. Thanks for the shared academic adventure, good company, and all the fun we had together. Special mention goes to Ida Morén, Luigia Brandimarte, Shuang Hao, Farzad Ferdos, and Andrea Betterle. Many thanks go to Aira Saarelainen, Marie Larsson, Britt Aguggiaro, and Merja Carlqvist for their active support in administrative matters.

I am grateful to Bijan and Shahrzad, who nourished me with their kindness, friendship, and morality. I was fortunate to meet you both during my early days in Stockholm.

I would like to thank my beloved parents and siblings. Mom and Dad, you both are the most valuable people in my life; you are my power, strength, and love. Without you, I might not be the person I am today. I am forever in debt to you. Azizi Zahra, Dadash Mohammad, Mojtaba, and Yasaman, thanks for your unconditional love. You should know that I am nothing without all of you.

Finally, my special thanks to my wife and best friend, Shiva, without whose love and constant support none of this work would have been possible. Thanks for your selfless love and filling my life with happiness. I am glad that we were together throughout my PhD journey, which made this time even more special.

Brian Babak Mojarrad

Stockholm, November 2021

TABLE OF CONTENT

LIST OF FIGURES

LIST OF TABLES

ABBREVIATIONS

HLRW	High-Level Radioactive Waste
DEM	Digital Elavation Model
SWI	Sediment Water Interface
LiDAR	Light Detection and Ranging
SWEREF99	Swedish Reference Frame 1999
SWEREF99TM	Swedish Reference Frame 1999 Transverse Mercator
a.s.l	above sea level
SGU	Sveriges Geologiska Undersökning
PCA	Principle Component Analysis
MLTS	Multi-Level Temperature Sticks
CDF	Cumulative Distribution Function
WTR	Water Table Ratio
QD	Quaternary Deposits
Re	Reynolds number (-)
ρ	Water density (kg/m^3)
Q	Volumetric flow rate (m^3/s)
d_h	Hydraulic diameter (m)
μ	Kinematic viscosity of the water (kg/(s.m))
A_{CR}	Cross sectional area of the medium (m^2)
V	Mean value of Darcy flow velocity within the porous medium (m/s)
K	Hydraulic conductivity (m/s)
H	Hydraulic head (m)
L	Distance (m)
Z_e	Bedform elevation (m)
p	Pressure (Pa)
g	Fravitational acceleration (m/s^2)
k_P	permeability (m^2)
v_{spg}	Seepage flow velocity through pores and fractures (m/s)
n	Porosity (-)
Z_B	Bed topography variation (m)
N	Number of wavelengths in Fourier series spectrum (-)
A	Amplitude coeffiecient of the topography fluctuation (m)
k	Wavenumber (m^{-1})
λ	Wavelength (m)
c	Empirical decay coefficient (m^{-1})
α	Anisotropy ratio (-)
H_S	Total hyporheic hydraulic head (m)
C_{damp}	Hydrostatic damping factor (-)
Fr	Froude number (-)

v_f	Stream flow velocity (m/s)
D_W	Stream water depth (m)
H	Total hydraulic head (m)
H_C	Catchment scale hydraulic head (m)
H_T	Cachment scale trend in water surface elevation (m)
K_D	Permeability at a specific depth (m^2)
D	Decay coefficient (m)
γ	Decay coefficient (m)
K_S	Permeability at the topography surface (m^2)
δ	Skin depth (m)
Δh	Groundwater heaping (m)
d	Difference between maximum terrain elevation and the mean level of surface water (m)
R	Infiltration rate (m/s)
L_W	Mean distance between the surface water resources (m)
m	Dimensionless coefficient (-)
D_T	Thickness of the aquifer (m)
α(Fr)	Flow regime coefficients in hydrostatic damping factor (-)
β(λ)	Wavelength coefficients in hydrostatic damping factor (-)
P_{WS}	Power spectra of the stream water surface elevation (m^2)
P_{BS}	Power spectra of the streambed topography elevation (m^2)
R_P	Ratio of power spectra (-)
i	Wavelength number is x direction (-)
j	Wavelength number is y direction (-)
$\sigma_{S,B}$	Standard deviation of fluctuation in bedform evaluation (m)
h_m	Velocity head amplitude (m)
W_C	Catchment scale groundwater flow vertical velocity (m/s)
W_S	Streambed scale hyporheic flow vertical velocity (m/s)
ξ	Coefficient in regression model (-)
C	Independent characteristic parameter
$t_{solutes}$	Solute transport time (s)
t_{spg}	Groundwater seepage travel time (s)
R	Retardation factor (-)
e	Elevation (m)
DS	Distance to the catchment outlet (m)
S	slope (-)
Z_Q	Soil depth (m)
SO	Stream Order (-)
$D_{HF,\,max}$	Maximum penetration depth of the surface water flow into the sediment (m)
τ	Residence time of hyporheic fluxes (s)
R^2	Coefficient of determination (-)

$R^2_{adj.}$	Adjusted coefficient of determination (-)
GtS	Gradient to stream (-)
SW_a	level of power spectral density water surface elevation (m)
SW_b	slope of power spectral density of water surface elevation (-)
MSC	Mean subcatchment size (m^2)
DW_{ff}	Darcy-weibach friction factor (-)
A_{sub}	Subcatchment area (m^2)
e_{std}	Standard deviation of landscape elevation (m)
EaS	elevation above stream (m)
L_{str}	Stream length (m)
S_{str}	Stream Slope (-)
$Z\text{-}str_{std}$	Standard deviation of elevation along the stream (m)
Q_{str}	Stream discharge (m^3/s)
U_{str}	Stream flow velocity (m/s)
A_{str}	Cross sectional area of stream channel (m^2)
W_{str}	Width of stream channel (m)
Str-P	Stream power (N/s)

ABSTRACT

Rivers and aquifers are continuously exchanging water, driven by processes that occur on various temporal and spatial scales, ranging from small streambed features to large geological structures. The interaction between these two components occurs in permeable sediments below the stream channel, called the hyporheic zone. This zone is an important ecotone in which water, energy, and solutes originating from groundwater and stream water mix. The exchange fluxes through the hyporheic zone are controlled by a distribution of hierarchically nested flow cells of different sizes that are generated by a spectrum of spatial scales of the hydraulic head condition. Thus, a multiscale mathematical approach is required to reach a comprehensive understanding of the hyporheic exchange processes. Therefore, this thesis investigates the roles of regional groundwater flow and hyporheic fluxes in a nested flow system within the streambed sediment. Next, the study assesses the importance of regional and local parameters in generalizing the surface water and groundwater interaction. This division of the top-boundary condition in two scale-intervals of the sub-surface flow is arbitrary but facilitates the analytical procedure. The regional groundwater flow field is evaluated using numerical modeling, accounting for the site-specific landscape morphology and geological heterogeneity of a Swedish boreal catchment. An exact spectral solution is applied to the hyporheic flow with account taken to local streambed topography fluctuation. Combinatorial sampling of the modeled flow data and a Monte Carlo simulation are used in a sensitivity analysis to address the uncertainty in hydrostatic and dynamic head contributions to the hyporheic flow field. Then, the impact of the regional groundwater and the hyporheic flows on the nested flow system in aquatic sediment are studied through superpositioning of the flow fields. This is an efficient approach to analyze the nested flow system because the impact on individual scale intervals can be evaluated separately. Additionally, the impacts of streamflow discharge intensity on hyporheic exchange flow fields are investigated through field investigation. In this study, the hyporheic fluxes velocity at the streambed interface were generally at least one order of magnitude higher than groundwater flow velocity. This reflects the domination of hyporheic fluxes at the streambed interface, leading to significant impacts on the discharge of deeper groundwater through the hyporheic zone. Significant effects were found in flow travel time, direction and discharge areas at the streambed sediment. Thus, the upward groundwater flow contracted near the streambed surface and discharged in a fragmented pinhole pattern at the sediment–water interface. The results also indicated that the magnitude of groundwater flow and the heterogeneity of the subsurface sediment (i.e., the depth decaying hydraulic conductivity of streambed sediment) controlled the depth of hyporheic exchange flow in aquatic sediment. Furthermore, the increased stream flow intensity led to a wide range of hyporheic flow residence times in which temperature was used to evaluate stream segments with gaining and losing conditions.

Keywords: groundwater flow, hyporheic zone, multi-scale modeling, spectral analysis, fragmentation of discharge zones, characteristic parameters

1 INTRODUCTION

Surface water and groundwater continuously exchange water, mass, and energy. The interaction between groundwater and surface water substantially influences the quality of water resources and plays an important role in water resources management programs. Therefore, a detailed understanding of groundwater–surface water interaction and the impact of each on the other is essential in describing the fate and transport of existing contaminants in the hydrosphere. This section provides a brief description of the water resources accounted for in this study, followed by environmental issues inspiring me to investigate the interaction between groundwater and surface water.

1.1 Groundwater

Groundwater is the water available in soil pores and fractures of bedrock materials within the Earth's crust. The subsurface domain can be both unsaturated and saturated, and the saturated domain extends several thousands of meters into the Earth. The groundwater table of the saturated domain (also called the phreatic surface) is the interface with atmospheric pressure that separates the saturated and unsaturated zones. Surface water (including springs, lakes, streams, and wetlands) are shaped where the groundwater table meets the ground surface. Groundwater table is dynamic and changes over time, an action that depends on the amount of groundwater recharge and discharge. Groundwater recharge results from infiltration at the ground's surface, and the discharge generally occurs in surface water bodies. The momentaneous ratio of groundwater recharge to groundwater discharge controls the rise and fall of the groundwater table. However, in wet climates, such as focused on in this thesis, the groundwater table is a subdued replica of the landscape topography. Groundwater movement results from a wide range of spatial scales of the landscape topography, and it carries chemicals and contaminants with various properties over these spatial scales. Additionally, the chemical composition of shallow groundwater is related to existing chemical compounds in precipitation, weathering products, and the microbial decomposition of organic material. On the other hand, the groundwater at a great depth, which is substantially slower than shallow groundwater, is highly saline and contains various types of solutes and contaminants.

1.2 Hyporheic Exchange Flow

The hyporheic zone refers to the sediment below and adjacent the river where the stream water and groundwater mechanically and chemically interact with each other. Orghidan (1959) used the term "hyporheic" for the first time in limnologic science by combining the Greek roots *hypo* and *rheos*, meaning "under the flow." Hyporheic flow is a subsurface flow originating from surface water that mixes with subsurface water coming from different origins and finally returns to streams (Harvey and Bencala, 1993). In the 1960s, scientists realized that solute transport in streams is affected by uptake in dead zones and transient storage, leading to the development of hydraulic and hydrologic aspects (Thackston, 1967; Thackston and Schnelle, 1970). This hydraulic–hydrologic research continued during the early 1980s, emphasizing one-dimensional model approaches (Bencala, 1983). Such research received extensive attention on a variety of different hydromechanical and biogeochemical processes during the subsequent decades (Cardenas, 2015). Hyporheic flow is distinct from groundwater due to its bidirectional flow, meaning the flow both begins and ends in the open stream water. Thus, exchange can occur in both directions across the streambed over spatial scales ranging in length from millimeters to several meters and beyond. Additionally, this hyporheic flow process is affected by groundwater discharge through the stream bottom of water generated by the infiltration-recharge mechanism occurring outside the stream's water continuum. Previous research conducted on hyporheic flow has often applied an integrated perspective of hydrology and biochemistry of the subsurface domain near the streambed interface (Stanford and Ward, 1993). Furthermore, many studies have investigated the impact of hyporheic exchange flow on water quality, river restoration, and the

ecology of streambed sediment (National Research Council, 2002; Kasahara et al., 2009; Boulton et al., 2010).

1.3 Motivation of the Thesis

Subsurface flow occurs on a wide range of spatial scales associated with hierarchically nested flow cells, from highly localized flows, like hyporheic fluxes, to very long groundwater flow paths originating hundreds or thousands of meters away (Toth, 1963). The main scientific question of this study is to what degree various subsurface flows occurring at different spatial scales influence the discharge of deep groundwater in streams and the hyporheic flow pattern. Addressing this question requires an analysis of the subsurface flow process to investigate how various spatial scales of the flow field form and what controls the flow directions and velocities. Previous studies have investigated different factors that influence the groundwater table and fluxes, including the effects of landscape topography, subsurface geology, and climate conditions (Tóth, 1970; Winter, 1999; Devito et al., 2005; Leach et al., 2017; Singh et al., 2019), but the impact of hyporheic flow on the regional groundwater discharge near the streambed surface has thus far been overlooked by researchers. Even so, multi-scale subsurface modeling allows one to consider the impact of the regional groundwater flow on the hyporheic flow, which has been previously investigated (Boano et al., 2008; Trauth et al., 2014; Fox et al., 2016). However, the associated flow with different ranges of individual spatial scales was loosely defined in previous studies (Cardenas and Wilson, 2007; Boano et al., 2009). Applying a multiscale modeling approach through subdividing the topographical features into individual spatial scales facilitates analyses of decoupled subsurface flow from various ranges of spatial scales. Hyporheic flow is induced by hydraulic head gradients originating from hydrostatic and dynamic pressure components, which arise from variability in the surface elevation and flow velocity of the water, respectively (Boano et al., 2014; Cardenas, 2015). Previous studies have estimated the hyporheic flow field using experimental and numerical analyses and have described the hyporheic flow field using the flow velocity variation over bedforms. However, the applied methods in hyporheic flow estimation generally neglect the role of variation in stream water elevation over the bedform (Marzadri et al., 2014; Caruso et al., 2016), which can be a limiting assumption. Recently, a few studies have investigated the role of stream discharge intensities on hyporheic flow (Wu et al., 2018; Singh et al., 2019). On the other hand, topography variation has been considered as the main factor affecting the subsurface flows in the hyporheic zone. However, a lack of high-resolution topographical data has introduced conceptual errors in quantifying the hyporheic flow fields. Consequently, this phenomenon has affected the quality of multi-spatial subsurface flow results and the validity of modeled hyporheic fluxes. In fact, it is to some extent impossible to account for all the spatial scales of subsurface flows in one single model. Therefore, one way to satisfy topography resolution demands would be to separate the multi-spatial flows problem into different scale intervals (spectra). Streambed morphologies show fractal structures (Rodríguez-Iturbe and Rinaldo, 1997), and the subsurface flow has a similar hierarchical pattern that is associated with the fractality of the landscape topography (Zijl, 1999; Wörman et al., 2007; Cardenas, 2008). Fractality of topography facilitates identification of the functional trends in landscape elevation by applying spectral analysis (Wörman et al., 2006) and rescaling topography to resolution intervals not necessarily covered by data. The latter operation is required for the hyporheic flow field modeling. In addition, the linearity of the groundwater flow equation enables the superpositioning of solutions for the separate topographical spatial scale intervals, which substantially facilitates the understanding of nested flow systems. However, the previous studies generally included a limited range of spatial scales in each model case, but utilization of the fractal trends offer the option of generalizing the spectral analysis of topography elevation over a much wider range. Thus, the present thesis establishes two separate models over different scale ranges for groundwater flow and hyporheic fluxes. In these models, the regional groundwater flow is quantified using numerical solutions, whereas the hyporheic fluxes are quantified by exact

solutions. Separating the spatial scale ranges in the modeling approach using numerical and exact solutions allows to consider various subsurface flow through the required topographical data resolutions. Finally, combing the two aforementioned subsurface flows increases the conceptual understanding of the importance of each spatial flow field and the flow process occurring within the streambed sediment.

Recent studies have highlighted the importance of interaction between groundwater and hyporheic fluxes for different scientific disciplines, including: hydrogeology and water resources management (Fleckenstein et al., 2010; Caruso et al., 2016); chemical and biological reactions (Boulton & Hancock, 2006; Landmeyer et al., 2010); and microbial metabolism (Zarnetske et al., 2011). All of these scientific subjects were studied during the PhD period, but the focus of this thesis is the following hydrogeological issues.

1.3.1 Groundwater–hyporheic flow interactions

Although groundwater and hyporheic fluxes are often considered to be separate subsurface flows, numerous studies have demonstrated the interactions between these two flows (Boano et al., 2014; Lewandowski et al., 2019). In particular, studies have shown that the hyporheic zone depth substantially decreases in the regions where groundwater discharge is intense. Thus, the solute transport times within the hyporheic zone are substantially impacted by both groundwater and hyporheic fluxes. Previous investigations have studied interactions between groundwater and hyporheic fluxes at the streambed sediment (Cardenas, 2015; Krause et al., 2011), but the impacts on size of the groundwater discharge flow have never been examined. The hyporheic fluxes typically have high oxygen contents and unstable temperatures due to the impact of diurnal temperature signal. On the other hand, groundwater flow often displays a low oxygen content and a relatively stable temperature. Mixing groundwater flow and hyporheic fluxes with different properties (e.g., temperature and oxygen content), along with the existence of various chemical, leads to various microbial metabolisms. These conditions can also cause a number of reactions, such as oxidation of organic carbon, denitrification, or bioremediation of organic carbon within the hyporheic zone (Duff and Triska, 1990; Conant et al., 2004; Nogaro et al., 2013). The variations in the size of the hyporheic upwelling regions at the streambed interface influence the aquatic habitat diversity and the stream's water quality (Poole et al., 2006). Previous studies have highlighted the controlling impacts of topography variations, geological formations, and climatic conditions on regional groundwater circulation and its discharge location. However, the role of hyporheic flow in regional groundwater discharge has often been neglected. This role is important for the retention of contamination and solutes transported by deep groundwater flow.

1.3.2 Radioactive dose assessment

The isolation of the high-level radioactive waste (HLRW) in deep geological formations (i.e., several hundreds of meters deep within bedrock) is one of the most recognized options for radioactive waste disposal. Radioactive dose assessment concerns the impact of leakage scenarios from HLRW repository in deep bedrock on the safety of the surface environment and human health. Additionally, a comprehensive understanding of the radionuclide transport in different geological formations (such as bedrock and soil strata) is critical for developing a safety assessment program. Since regional groundwater controls water flow at the repository depth, the regional groundwater is the main component in radionuclide transport. Therefore, it is essential for those involved to understand regional groundwater flow travel time in different geological formations and the behavior of the flow at the discharge zones. That is, such knowledge is crucial in long-term safety assessments. For instance, research conducted in Sweden mainly focused on the radionuclide transport via large-scale groundwater flow field from a repository located in deep bedrock, applying the results as input to biosphere models (SKB, 2004). Large-scale groundwater model provides the required information to estimate the deep groundwater discharge pattern at the geosphere–biosphere interface which are used in the radiation safety assessment of the ecological models (Hedin, 2006). Radionuclide accumulation and transport

close to the landscape topography surface are of great concern from the safety assessment perspective. In particular, the existence of radionuclide compounds in streambed sediment and Quaternary deposits significantly increase the risk of harmful radiation threating the safety of human beings and other living biota. The overall deep groundwater flow travel time in Quaternary deposits and streambed sediment is pertinent to the safety assessment because it reflects the maximum exposure time of human bodies and the surface environment to radionuclide radiation. Previous literature has studied the radionuclide mitigation in bedrock and Quaternary deposits at various depths of radioactive waste disposal (Holmén et al., 2003; Ericsson et al., 2006; Marklund et al., 2008). However, none of these studies investigated the detailed flow behavior of the discharge zone, namely the importance of how the regional scale flow field and hyporheic fluxes influence each other's velocity and flow direction. That is, the interaction between hyporheic exchange fluxes and subsurface groundwater flow influences the fate and transport of radionuclide contaminants between surface water and aquifer and controls the water quality and biological activities within the streambed sediment (Stanford & Ward, 1988; Vervier, 1990; Medina et al., 2004).

1.4 Objectives

The main aim of this thesis is to investigate how the hyporheic flow and groundwater influence each other within the discharge zone arising in streambed sediments. The research was conducted by applying numerical modeling and field investigations. In particular, the impact of hyporheic exchange fluxes and subsurface groundwater flow on each other was investigated through a complex multiscale modeling approach. Beyond this, the role of temporal variation in surface water level on the hyporheic flow field was studied via field experiment and numerical modeling. Specific study site data were used throughout the investigation so that the numerical models reflected the real watershed. However, different types of sensitivity analysis were used during the investigation to generalize the results for a broader range of catchment's characteristics. Furthermore, this thesis addresses the role of hyporheic exchange fluxes in subsurface nested flow modeling. Therefore, the estimation of the hyporheic exchange fluxes and the parameter affecting its magnitude were investigated in detail. The uncertainty in hyporheic flow results was addressed by applying either a combinatorial sampling approach or Monte Carlo simulations. Additionally, this thesis provides a new approach to define a digital elevation model (DEM) of the groundwater table, which satisfies the natural infiltration condition of the area as well as topographic controls of surface water objects. The overall aim is to provide insight into the importance of hyporheic exchange fluxes in regional groundwater solute and contamination transport near the bed surface. In turn, such data could be used to derive an improved conceptual view of surface water–groundwater interactions.

The detailed aims of this thesis are as follows:

- To estimate the impacts of regional scale groundwater flow on the hyporheic exchange fluxes (Paper I),
- To quantify the impact of variation in the stream discharge on hyporheic exchange fluxes via field investigation and numerical modeling approaches (Paper II),
- To parametrize a biosphere compartment model for the fate and transport of radionuclide compounds in the biosphere (Paper III),
- To investigate the major impacts of hyporheic exchange fluxes on regional groundwater flow field beneath the deep groundwater discharge points (Paper IV), and
- To investigate the role of geographic and hydrogeologic factors on the interaction between groundwater and hyporheic flows (Paper V).

2 THEORY OF SUBSURFACE FLOW PROCESS

The following section describe the theoretical knowledge applied in the modeling approach. In particular, this section expresses the dominant flow equations in the subsurface domain.

2.1 Groundwater Flow in Saturated Porous Media

The groundwater movement in porous media is controlled by the gradient in the hydraulic head, in which the flow regime could be either laminar or turbulent based on the flow's ratio of inertial forces to viscous forces. Reynolds number is used to quantify this ratio:

$$Re = \frac{\rho Q d_h}{\mu A_{CR}} = \frac{\rho v d_h}{\mu} \quad (1)$$

where ϱ (kg/m^3) is the water density; Q (m^3/s) is the volumetric flow rate per cross-sectional area; A_{CR} (m^2) is the cross-sectional area of the medium; d_h (m) is the hydraulic diameter in which it represents grain diameter for the porous media; μ (kg/(s.m)) is the kinematic viscosity of the water; and v (m/s) is the mean value of flow velocity (the Darcy velocity for the flow within the porous medium, defined as Q/A_{CR}). The flow is considered to be laminar for Re<1, while the Reynolds number at approximately 100 or above reflects the fully turbulent flow regime (Bear, 2012). Additionally, the flow begins to transition from a laminar to a turbulent flow, whereas the Re number increases from 1 to 100. This range refers to the flow with a transition state. The natural groundwater flow regime within the subsurface domain is laminar, where the flow is governed by Darcy's law:

$$v = \frac{Q}{A_{CR}} = -K \frac{\partial H}{\partial L} \quad (2)$$

where K (m/s) represents the hydraulic conductivity, H (m) is the hydraulic head, and L (m) is the distance. The hydraulic head consists of elevation, velocity, and pressure heads, and the velocity head is often neglected in groundwater hydrology, as displayed in the following equation:

$$H = z_e + \frac{P}{\rho g} \quad (3)$$

where z_e (m) is the elevation, P (Pa) is the pressure, and g (m/s^2) is the gravitational acceleration. The hydraulic conductivity depends on the properties of the fluid and porous media, including permeability, fluid density, and kinematic viscosity:

$$K = k_p \frac{\rho g}{\mu} \quad (4)$$

where k_P (m^2) is the permeability of the porous media. The density and kinematic viscosity of water substantially depend on the water temperature and its salinity. Consequently, the hydraulic conductivity of the subsurface domain varies, resulting in a heterogeneous domain. Therefore, the Darcy's velocity is expressed as:

$$v = -K_x \frac{\partial H}{\partial x} - K_y \frac{\partial H}{\partial y} - K_z \frac{\partial H}{\partial z} \quad (5)$$

The Darcy flow velocity is described as the mean flow velocity over a cross-sectional area of the porous medium (including both grains and pores). However, the flow velocity through pores and fractures can be estimated using the seepage velocity:

$$v_{spg} = {}^{v}/_{n} \quad (6)$$

where v_{spg} (m/s) is the seepage velocity, and n (-) represents the porosity of porous medium. On the other hand, the continuity equation for incompressible flow under the steady state condition is described as follows:

$$\frac{\partial v_x}{\partial x} + \frac{\partial v_y}{\partial y} + \frac{\partial v_z}{\partial z} = 0 \quad (7)$$

Combining Darcy's law (Equation 5) with the continuity equation (Equation 7) leads to governing equation for three-dimensional steady-state groundwater flow:

$$\frac{\partial}{\partial x}\left(-K_x\frac{\partial H}{\partial x}\right)+\frac{\partial}{\partial y}\left(-K_y\frac{\partial H}{\partial y}\right)+\frac{\partial}{\partial z}\left(-K_z\frac{\partial H}{\partial z}\right)=0 \quad (8)$$

2.2 Hyporheic Exchange Fluxes

Hyporheic flow is a reciprocal flow below the streambed interface that plays a significant role in biogeochemical processes. Hyporheic flow is induced by hydraulic head gradients originating from hydrostatic and dynamic pressure components. These elements arise from variability in the streambed surface elevation and the near-bed flow velocity, respectively, effects induced by streambed topography. Both landscape and streambed topography fluctuation have demonstrated fractal behavior (Rodríguez-Iturbe and Rinaldo, 1997; Turcotte, 1997), which can be represented by a real Fourier series through a nearly constant power law relationship between amplitudes and wavelengths of topography elevation from continental to streambed scales (Wörman et al., 2007). This constant power law suggests the generalization of the topography data outside the interval of the observational data. Beyond this, the hierarchical nested flow cells induced by large-scale groundwater flow are controlled by landscape topography variation under wet climate conditions (Toth, 1963). In particular, the groundwater flow is controlled by a fractal scaling of the landscape topography when the infiltration rate (from precipitation) is higher than the hydraulic conductivity of the soil. Domination of this condition often allows one to assume that groundwater levels follow topography variations in a quasi-steady-state condition. Zijl (1999) derived an exact solution to groundwater flow circulation for regions with topography-controlled groundwater flow. Furthermore, the fractal behavior of landscape topography can be related to groundwater flow field using a three-dimensional, exact solution (Wörman et al., 2007). This solution was enhanced by Cardenas and Jiang (2010) and Marklund and Wörman (2011) to include anisotropy and heterogeneity in subsurface geological formations, such as depth-decaying hydraulic conductivity. Additionally, the application of a Fourier series can represent the observed topography data as follows:

$$Z_B(x,y)=\sum_{j=1}^{N}\sum_{i=1}^{N}\left(A_{i,j}\right)_B\, sin(k_i x)\, cos(k_j y) \quad (9)$$

where Z_B (m) is the bed topography variation, N (-) is the number of wavelengths in the applied Fourier series spectrum, A (m) is the amplitude coefficient of the topography fluctuation, $k=2\pi/\lambda$ (m^{-1}) is the wavenumber, and λ (m) is the wavelength. Equation 9 divides the observed topography into sets of harmonic functions with specific amplitudes and wavelengths. The distribution of topographic amplitudes across wavelengths follows this equation (Turcotte, 1997):

$$A_B = a \times \lambda^b \quad (10)$$

where a (-) and b (-) are the coefficients. The fractal nature of topography facilitates consideration of the same power law between amplitudes and wavelengths for shorter wavelengths than those for which observations are conducted. Hence, the topography elevation data can be rescaled into finer resolutions (representing streambed variations) that suit the hyporheic flow modeling (Figure 1; $A_{i,j}$ is determined from data, and the figure shows the marginal distributions). The groundwater flow circulation and the landscape elevation display identical fractal natures under wet climate conditions. Therefore, the hyporheic hydraulic head is assumed to closely follow the streambed variation, and this head can be divided into hydrostatic and dynamic contributions. Both hydrostatic and dynamic components of the hyporheic hydraulic head can be estimated using the stream water elevation. The hydrostatic hydraulic head is water surface elevation and is due to fully stagnant surface water due to gravitational forces, whereas the dynamic hydraulic head is the additional pressure due to the flow velocity over a bedform. The hydrostatic hydraulic head can be represented by a smoothed version of topography variation (Marzadri et al., 2014), which itself can be illustrated by a scaling or damping factor that varies with Froude number (i.e., flow regime) and the wavelength of the Fourier series spectrum. Similarly, the dynamic component of the hyporheic hydraulic head can be represented by a scaling or damping factor that depends on streambed topography fluctuation and the physical characteristics of the stream

water (i.e., flow velocity and water depth) (Fehlman, 1985). Detailed descriptions of the hydrostatic and dynamic components of the hyporheic hydraulic head are presented in Section 3.3.1. Additionally, hydraulic conductivity is anisotropic, where in this study, anisotropy was aligned with the horizontal surface, reflecting the exponential decay of hydraulic conductivity only with depth (Saar & Manga, 2004; Marklund & Wörman, 2011). These facts imply an additional damping of the hyporheic hydraulic head induced by depth decaying hydraulic conductivity.

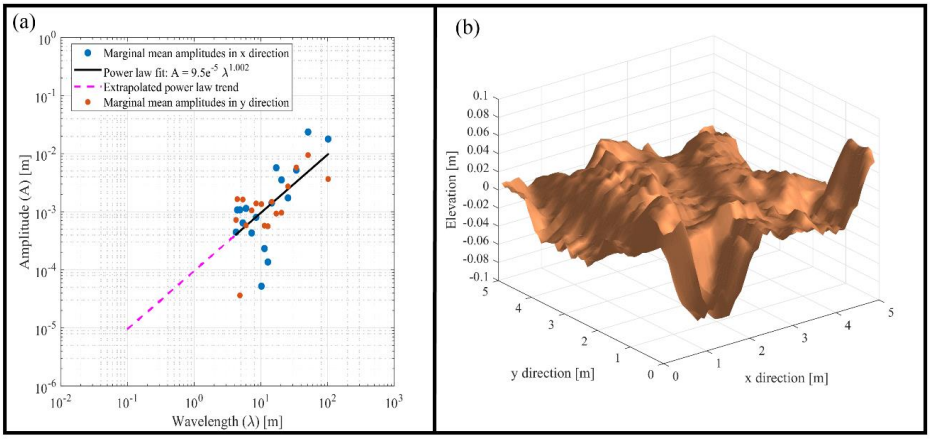

Figure 1. (a) Marginal amplitude spectra based on the topographical data for one of the 100 m × 100 m regions and the extrapolated power law trend for rescaling; (b) Rescaled topography for one of the selected regions (5 m × 5 m with 0.1 m × 0.1 m resolution) (Paper I, III, IV)

Finally, the total hyporheic hydraulic head can be represented by the following equation:

$$H_S(x,y,z) = \sum_{j=1}^{N}\sum_{i=1}^{N}\left[C_{damp}(Fr,\lambda_i) + \left(\frac{h_m}{\sigma_{S,B}\sqrt{2}}\right)\right](A)_{i,j}\sin(k_i x)\cos(k_j y)\times e^{\left(-\frac{c}{2}+\sqrt{\frac{c^2}{4}+\alpha\left(k_i^2+k_j^2\right)}\right)z} \quad (11)$$

where H_s (m) is the total hyporheic hydraulic head, C_{damp} (-) is the hydrostatic damping factor reflecting the ratio of surface water fluctuation to streambed topography fluctuation, $Fr = \frac{v_f}{\sqrt{gD_w}}$ is the Froude number, v_f (m/s) is the stream flow velocity, D_w (m) is the stream water depth, g (m/s^2) is the gravitational acceleration, $\left(\frac{h_m}{\sigma_{S,B}\sqrt{2}}\right)$ is the dynamic head coefficient, c (m^{-1}) is an empirical decay coefficient, and $\alpha = \frac{K_x \text{ or } K_y}{K_z}$ (-) is the anisotropy ratio.

2.3 Separation of Multiscale Subsurface Flow on Scale Intervals

Groundwater–surface water interaction occurs across a wide range of spatial scales, from centimeters to hundreds of kilometers. Regional groundwater flow circulates hundreds or thousands of meters within the subsurface domain, whereas hyporheic fluxes spatial scale ranges are in centimeters or meters. Due to the significant size difference between the circulation cells of hyporheic fluxes and regional groundwater flow fields, a multi-scale modeling approach is required to investigate the mutual impacts of these factors. The linearity of Equation (8) and the

assumption of the same boundaries allows one to apply superposition principle to separate the total hydraulic head H(x,y,z) into individual terms as follows:

$$H(x,y,z) = H_S(x,y,z) + H_C(x,y,z) + H_T(x,y) \quad (12)$$

where $H_S(x,y,z)$ is the hyporheic hydraulic head fluctuation (i.e., detrended hyporheic huydraulic head); $H_C(x,y,z)$ is the catchment-scale hydraulic head fluctuation; and $H_T(x,y)$ represents the catchment-scale trend in water surface elevation (Figure 2). The separation between the hyporheic and catchment-scale hydraulic head is arbitrary, implying that these entities represent different scale intervals that, in principle, do not overlap. Therefore, two distinct spatial-scale models can be used separately to represent the combined flow field of the hyporheic exchange flow ($H_S(x,y,z)$) and the regional scale groundwater flow field ($H_C(x,y,z)+H_T(x,y)$). This combined flow field is important for estimating the effects on the deep groundwater discharge as well as the hyporheic flow behavior.

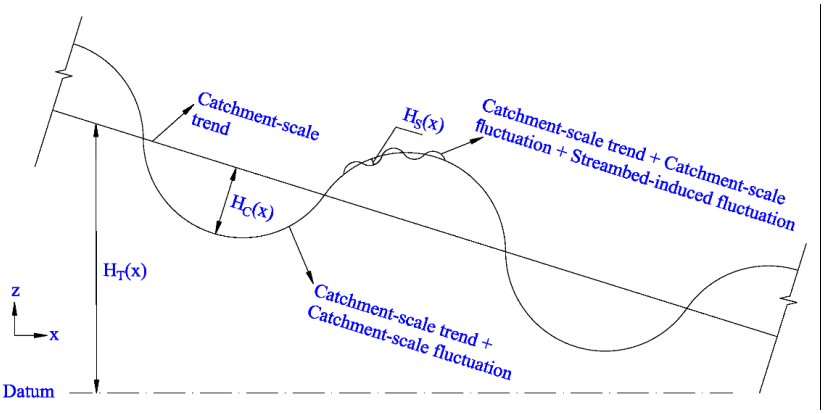

Figure 2. Conceptual sketch of the total hydraulic head (H) components along a surface water pathway: hyporheic scale, $H_S(x)$, catchment scale, $H_C(x)$, hydraulic head fluctuations, and the trend in the catchment-scale water surface elevation, $H_T(x)$ (Paper I)

2.4 Hydrogeology

The variations in the spatial geological properties of the subsurface domains cause variations in soil properties in both the horizontal and vertical directions. In particular, the heterogeneity of hydraulic conductivity in Quaternary deposits reflects the availability of different soil types in the watershed. Additionally, bedrock fracture size and the porosity of the subsurface domains decrease in depth with increasing stress from above soil depth. This phenomenon leads to a permeability reduction with depth for most geological formations. Previous studies have indicated a nonlinear decay behavior with depth for various regions with different geological properties (Streltsova, 1987; Lee & Farmer, 1993; Williams et al., 2006; Jiang et al., 2009). Ingebritsen and Manning (1999) used geothermal data and metamorphic systems to suggest a power-law function for the depth decay permeability:

$$k_P(z) = k_D \left(\frac{-z}{D}\right)^{-\gamma} \quad (13)$$

where k_P (m^2) is the permeability, k_D (m^2) is the permeability at a specific depth, and D (m) and γ (m) are the decay coefficients. Ingebritsen and Manning proposed that $K_D=10^{-14}$, D=1000, and γ=3.2 represent the Earth's crust. A few years later, Saar and Manga (2004) improved the depth-decaying permeability function representing the top 800 meters of the subsurface domain with an exponential function:

$$k_P(z) = k_s e^{z/\delta} \quad (14)$$

where k_s (m^2) is the permeability at the topography surface, and δ (m) is the skin depth suggested, with a value in the range of 200–300 m. Additionally, Morén et al. (2017) conducted a field experiment in a small Swedish stream (Tulltorps Brook) that measured the hydraulic conductivity of the stream bed sediment at two different depths (3 and 7 cm) for 58 points along the stream network (a 5800 m reach with an interval of 100 m). They discovered that the hydraulic conductivity of streambed sediment decays exponentially with depth where the empirical decay coefficient (1/δ) can be quantified experimentally.

2.5 Topography-Controlled vs. Recharge-Controlled Regional Groundwater Flow

Solving the groundwater flow problems in unconfined aquifers requires prior knowledge of the location of an area's free-water surface. Essentially, gravity is the main force for groundwater flow in a subsurface domain in which the variations in topography elevation and the geological properties of the subsurface regions control the gravitational impact on the flow. In particular, Haitjema and Mitchell-Bruker (2005) assumed that a water table follows the landscape topography. In regions with humid climates and shallow Quaternary deposits, the groundwater surface closely follows the topography variations, so groundwater flow is controlled by topography. However, although the correlation between topography variation and groundwater surface was observed (Low et al., 2002; Peck & Payne, 2003), many previous studies have revealed a weak connection between water surface and topography elevation for certain hydrologic conditions (Desbarats et al., 2002; Blazkova et al., 2002; Shaman et al., 2002). Haitjema and Mitchell-Bruker (2005) developed a dimensionless ratio to distinguish topography-controlled regions from recharge-controlled regions. This ratio is called the water table ratio (WTR) and is expressed as follows:

$$WTR = \frac{\Delta h}{d} = \frac{RL_W^2}{mKD_T} \tag{15}$$

where Δh (m) is the groundwater heaping, d (m) is difference between maximum terrain elevation and the mean level of surface water, R (m/s) is the infiltration rate, L_W (m) is the mean distance between the surface water resources, m (-) is a dimensionless coefficient (can be either 8 or 16 depending flow direction), K (m/s) is the hydraulic conductivity, and D_T (m) is thickness of the aquifer. The region is classified as topography controlled for $WTR \geq 1$. On the other hand, $WTR < 1$ reflects the higher impact of groundwater recharge (on groundwater flow) than that of topography, and hence classified as the recharge-controlled region. Several investigations used the observed water table in boreholes to apply an interpolation method to estimate the groundwater surface for the whole catchment (Desbarats et al., 2002). However, this interpolation method did not consider the existing geological formations within the area, the local slope variation, or the depth of the soil layer. Regions with topography-controlled groundwater flow can often be represented using a subdued replica of the digital elevation modeled data (DEM) of the landscape topography as the water surface elevation. Furthermore, recharge-controlled groundwater flow models suffer from the knowledge required regarding the spatial distribution of infiltration in the unsaturated zone and the lack of datasets for evapotranspiration from vegetation (Marklund, 2009). The groundwater table in a humid climate (which is generally controlled by topography) is represented as a subdued, smoothed replica of the landscape elevation. However, the correlation between landscape elevation and groundwater surface may spatially vary due to infiltration. Thus, the groundwater table is topography-controlled for surface water resources (e.g., lakes, streams), whereas infiltration controls the groundwater level at high local landscape elevations (Desbarats et al., 2002; Sanford, 2002). Previous literature has demonstrated the controlling impact of DEM resolution on infiltration when decreasing the resolution (i.e., using a coarser DEM file) leads to decreased infiltration (Marklund and Wörman, 2011; Wang et al., 2018). Therefore, the realistic boundary condition can be numerically simulated through setting the landscape elevation at groundwater discharge areas (i.e., lakes and streams), but smooths (increasing mesh size) over the rest of the domain to constrain the model with measured infiltration. The aforementioned

method helps to set the Drichlet and Neumann boundary conditions at groundwater discharge (i.e., lakes and streams) and recharge (i.e., the rest of the domain) regions, respectively.

3 MATERIALS AND METHODS

This chapter presents the study catchment, data, and the methods applied throughout this PhD project. A numerical modeling approach and exact solutions were used to simulate the groundwater flow and hyporheic fluxes, respectively. The applied exact solution was employed due to the lack of high-resolution data, which are required for hyporheic flow modeling. Additionally, a field investigation was conducted on one of the subcatchments at the study site to evaluate the impact of stream flow discharge intensity on hyporheic exchange flow using the observational data (Paper II). In addition, five different Swedish catchments were used in Paper V to study the impacts of various topographic and hydrageomorpholocal factors on groundwater–surface water interaction.

3.1 Site Description

This section presents detailed information of the study sites that were used in this thesis. The Krycklan catchment was used in Papers I–V, whereas four additional Swedish catchments were used in only Paper V.

3.1.1 Krycklan catchment

The Krycklan research catchment (64°14' N, 19°46' E) is located near the City of Umeå, northwest of Sweden with an area of 68 km^2 (Laudon et al., 2013). This catchment is a well-monitored catchment, where different types of data sets have been collected for more than 50 years. The land use of the catchment is dominated by forestry, and a large portion of the catchment has been protected for almost a century. The stream discharge of the Krycklan catchment was first recorded in 1981. Currently, there are 15 stations within the catchment boundary that record the stream discharge in hourly resolution (Figure 3a). In this study, the streambed morphology of the stream channels was measured, and the physical characteristics of the stream channels were classified into 13 different groups (Laudon et al., 2013). The Krycklan catchment is characterized by a cold, humid climate, and the landscape is covered by snow throughout the entire winter. The average temperature of the Krycklan over the last 30 years was 1.8 °C, in which the highest and lowest temperature occurred during July (14.7 °C) and January (-9.5 °C), respectively (Laudon et al., 2007). The mean annual precipitation (from 1981 to 2010) of the catchment was 726 mm/y, from which half of the amount was estimated as runoff (382 mm/y), and the rest was annual mean evapotranspiration (344 mm/y; ©Swedish Meteorological and Hydrological Institute, SMHI). Approximately half of the precipitation (35–50%) fell as snow, which lay on the ground for approximately 167 days per year (Laudon & Löfvenius, 2016). Additionally, the Krycklan catchment is mostly covered by till, silty sandy sediment, and silty clay soil types. Silty clay and glacial sediment are mostly located along the stream network of the catchment (©Sveriges geologiska undersökning; ©Lantmäteriet, 2016). Additionally, bedrock outcrop, glacial sediment, lake sediment, and peat have covered small regions within the catchment (Figure 3a). The bedrock of the catchment includes Svecofennian gneissic bedrock with metasediments covered by Quaternary deposit containing tills in highland regions. This bedrock gradually changed to sandy sediment (up to tens of meters depth) toward the downstream of the catchment (Lyon et al., 2011; Leach et al, 2017). Sterte et al. (2018) developed a catchment scale numerical model of groundwater flow for the Krycklan catchment and calibrated the hydraulic conductivity values of the different soil types (used in Papers I–V). Light detection and ranging (LiDAR) measurement was conducted on the whole catchment to provide the digital elevation model (DEM) data for the land surface. The DEM file has a resolution of 2 m and 1 cm for the horizontal and vertical directions, respectively. The Swedish Reference Frame 1999 SWEREF99 was applied at the national level. The maps of the study domain are based on a

Transverse Mercator grid of this system, which is called SWEREF99TM. The highest elevation is 405 m above sea level (a.s.l), observed at the northeastern region of the catchment, whereas the minimum topography is 117 m a.s.l at the catchment outlet. The bedrock surface elevation had a 10-m resolution and has been quantified using the boreholes information (©Sveriges geologiska undersökning, SGU). The topography elevation ranges from 231 to 306 m a.s.l. between discharge Stations 5 and 6 of the Krycklan catchment, where most of field investigations at Krycklan catchment were conducted for Figure 3b (Paper II).

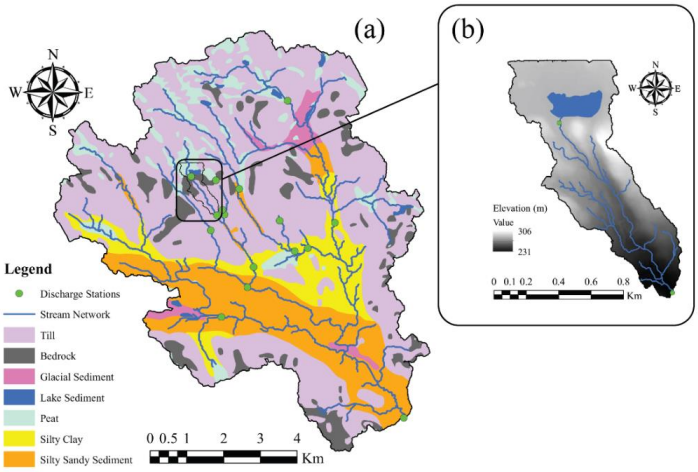

Figure 3. (a) The Krycklan catchment map, along with available soil types, stream network, and discharge stations (Paper I-V); (b) The experimental subcatchment between Discharge Stations 5 and 6, the topography elevation range, the existed river network, and the lake sediment within the subcatchment (Paper II)

3.1.2 Additional catchments

In addition to the Krycklan catchment, which was used in all the papers of this thesis, Paper V also used the Bodalsån (59°62' N , 18°60' E); Sävaån (59°50' N, 17°20' E); Tulltorpsån (55°28' N, 13°13' E); and Forsmarkån (60°22' N, 18°04' E) catchments. Forsmarkån is considered to be a forested catchment, whereas Bodalsån, Sävaån, and Tulltorpsån represent forested or agricultural regions. The mean annual discharge at the outlet of catchments, modeled by the Swedish Meteorological and Hydrological Institute (SMHI), vary between 0.63 m^3/s and 1.54 m^3/s for the four additional considered catchments in Paper V of the thesis (Bodalsån: 0.63 m^3/s, Sävaån: 1.54 m^3/s, Tulltorpsån 0.73 m^3/s, Forsmarkån 0.65 m^3/s). All of the additional considered catchments in Paper V have relatively similar yearly average precipitation to the Krycklan, where the mean annual precipitation is always in the range of 600–700 mm (Bodalsån: 662 mm/year, Sävaån: 612 mm/year, Tulltorpsån 686 mm/year, Forsmarkån 667 mm/year). Furthermore, the depth of soil layers vary among the catchments. For instance, the Bodalsån and Forsmarkån catchments are shallower than the others (soil depth less than 5 m). Tulltorpsån has the deepest Quaternary deposits among all the considered catchments in this thesis (i.e., greater than 20 m soil depth), and Sövaån has a soil layer in the range of 5–20 m of depth (Sridhar, 2020). Additionally, the landscape topography elevation represented flat (Sävaån, Forsmarkån) and relatively moderate (Bodalsån, Tulltorpsån) topographical elevations.

3.2 Numerical Model

The numerical modeling was conducted to analyze the hierarchically nested groundwater flow process in the Krycklan research catchment and subcatchment. The numerical model evaluated the variation in groundwater flow velocity and direction due to local and regional topography

elevation fluctuation as well as the heterogeneity of the subsurface domain. In particular, the groundwater exchange (i.e., discharge) velocity along the stream network was estimated, and the relation between flow velocity and stream order was discussed (Paper I). Additionally, the deep groundwater flow velocity (coming from 500 m depth from the surface) was evaluated within bedrock, Quaternary deposits, and streambed sediment and its discharge zones at the topography surface were assessed (Paper IV, V). The aims of the study were achieved via a numerical modeling of the Krycklan catchment containing various layers representing different geological properties with a variable numerical mesh size. The finite element method was used to numerically solve the groundwater flow equations. The impact of heterogeneity of subsurface soil on groundwater flow velocity was investigated by applying two different types of hydraulic conductivity in the numerical model of the field experimental reach: constant and heterogeneous hydraulic conductivities of soil (Paper II). The variation in geological properties of the subsurface domains were considered according to existing subsurface materials (i.e., sediment, soil, bedrock) where the depth-decaying hydraulic conductivity of each subsurface domain was considered (Papers I, III, IV, V).

The numerical model in Paper IV investigated the impact of the DEM resolution of the groundwater table when applied as the head boundary condition on the magnitude of the groundwater recharge. By adjusting the resolution, it was possible to fulfil the infiltration constraint corresponding to the observed data. Decreasing the resolution led to a smoothing of the groundwater table and a lower average groundwater flux at the surface, and the reverse occurred when increasing the resolution. Hence, the variable DEM resolution of the groundwater table helped to satisfy both the Dirichlet and Neumann boundary conditions in a single model. This part of the study was conducted using a finer DEM resolution at upwelling regions following the landscape topography and a coarser DEM resolution representing the groundwater table over the rest of the catchment.

3.2.1 Groundwater model setup

The groundwater flow modeling was conducted using the subsurface flow package in the COMSOL Multi-Physics software®. The groundwater flow model consisted of bedrock, Quaternary deposits, and streambed sediment as well as a description of topography and bedrock surface elevations. An equivalent continuum model was used for the bedrock domain in the numerical modeling approach, and the Quaternary deposit were represented based on the soil type map. Darcy's law was used to solve the groundwater flow equation in steady state condition through a finite element method. Thus, Equations 5 and 7 were solved using a numerical approach in the modeling framework. Depending on the hypothesis and the availability of the required data, 2D and 3D modeling were conducted (2D in Paper II and 3D in Papers I, III, IV, and V). The heterogeneity in hydraulic conductivity of Quaternary deposits was considered using the soil type map and the estimated values from previous literature on the Krycklan catchment (Sterte et al., 2018). Additionally, depth-decaying hydraulic conductivity was considered with exponential functions (Equation 14) for different layers of the model (Figure 4).

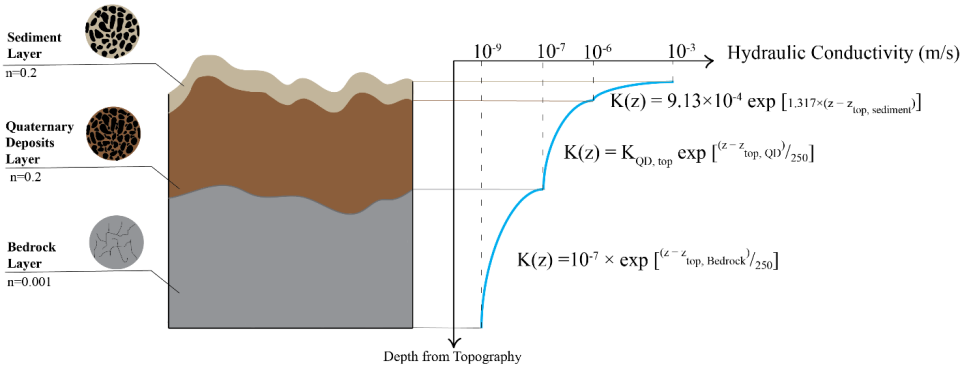

Figure 4. Conceptual sketch of the considered porosity, n, and depth-decaying hydraulic conductivity, K, for different layers of the model, in which QD stands for Quaternary deposits

A non-uniform numerical mesh was applied in the modeling approach, in which the mesh size decreased toward the topography surface, particularly with local elevation variation. The bottom flat surface of the model was assumed to be a no-flow boundary, whereas the lateral surfaces of the rectangular domain were considered as constant head boundary. The modeling was classified as a topography-controlled groundwater flow (i.e., the Dirichlet condition), meaning the groundwater surface followed the variation in landscape topography elevation (Paper I, III, V) but with possibilities for smoothing so that the infiltration or recharge condition of the area was also satisfied (Paper IV). To satisfy the natural infiltration (Neumann condition), the study employed a variable DEM resolution for the upward and downward regions at the surface. Additionally, this operation was conducted to satisfy the infiltration constraint (Paper IV).

3.2.2 Particle tracing in regional groundwater

Papers III, IV, and V concern the fate of deep groundwater flow in various subsurface strata coming from possible repository locations in deep bedrock, especially including the behavior of the discharge in surface water. Particle tracing helps to estimate the various characteristics of groundwater flow, such as velocity and travel time, and determine the discharge locations of the deep groundwater flow at the topography surface. Thus, a particle tracing was conducted by releasing 10,000 inert particles at the depth of the possible repository location (500 m beneath the minimum topography elevation). The particles were initially distributed in a 100×100 uniformly spaced grid over a flat surface. The particle tracing was conducted using the calculated seepage velocity consistent with Darcy's law, which describes particle motion in terms of travel times and trajectories. The inert particle travel time distribution in each subsurface domain was evaluated using the seepage velocity, for which the travel time of groundwater flow through the subsurface pores, and fractures were estimated (Equation 6). Furthermore, due to sorption and diffusion processes, the transport times for reactive solutes, such as radionuclides, in subsurface strata are higher than those of the groundwater flow seepage travel time. This leads to the retardation and retention of solutes in subsurface domains over a certain time period. Therefore, a retardation factor is often added in the solute transport process. In this study, the radionuclide transport was evaluated for ^{135}Cs within the subsurface strata using $t_{solutes} = (1 + R) \times t_{spg}$, where $t_{solutes}$ (s) and t_{spg} (s) are the solute transport time and groundwater seepage travel time in different subsurface domains, respectively. Additionally, R (-) is the retardation factor in which the values for bedrock and Quaternary deposits and sediment were $R_{rock} = 10$ and $R_{QD,\ sediment} = 500$ (Wörman et al., 2004; Jakubick, 1979; Neretnieks, 1979). Finally, the particles were traced until

they reached the topography surface or left the modeling domain. Papers III and IV considered only the deep groundwater particles that eventually reached the topography surface.

3.3 Spectral Exact Solution

The fractal distribution of topography fluctuation of both landscapes and streambeds provided the means to generalize the topography surface to a finer resolution over large streambed networks for the available data. The spectral approach applied here divided the topography variations into sets of harmonic functions with a power law between amplitudes and wavelengths (Equations 9 and 10). Holding the same power coefficient for the entire wavelength interval facilitates rescaling the topography surface. The variations in the dynamic and hydrostatic components of the hydraulic head along the bed surface follows the streambed topography fluctuations but are also affected by the hydrostatic damping factor and the dynamic coefficient (Equation 11). Therefore, the rescaled Fourier series representation of the topography combined with the hydraulic conductivity of the streambed sediment and stream flow velocity provide an exact solution of the three-dimensional hyporheic fluxes induced by streambed topography variation.

This analytical solution was used in Papers I, III, IV, and V. However, the applied exact solutions to hyporheic flow fields in the analysis were improved throughout this study. In particular, the first version was applied based on the assumption of homogeneous hydraulic conductivity with a fixed depth of the hyporheic model (Paper I, III). Next, the exact solution was improved, and a depth-decaying hydraulic conductivity was assumed based on an exponential decay function that was assessed from limited field data (Paper IV, V). Additionally, various types of sensitivity analysis were applied to account for the existing uncertainty in estimating the hydrostatic and dynamic head contributions.

The analytical solution was used to evaluate the hyporheic flow fields in the discharge locations for the deep groundwater, which could not be estimated due to lack of observational data over the stream network. Beyond this, the evaluated hyporheic flow field was required to investigate the impact of hyporheic fluxes and regional groundwater flow on each other's characteristics (e.g., velocity, flow direction) near the stream water interface. Additionally, the contributions of the hydrostatic and dynamic head components in the total hyporheic hydraulic head were studied to highlight the importance of water surface elevation and surface water velocity under different flow regimes.

3.3.1 Hydrostatic and dynamic head components of hyporheic flow fields

The hyporheic flow field depends on the contributions of the hydrostatic and dynamic head components over the streambed surface (Equation 11). The hydrostatic head component defines the variation in surface water elevation, which is different from the streambed topography fluctuation. The hydrostatic head component can be estimated by introducing a damping factor in bedform fluctuations. This damping factor is the ratio of stream water surface deviation to streambed surface deviation in comparison to mean elevations. Specifically, the damping factor depends on the wavelengths of the harmonic topography function and the flow regime. For example, at large wavelengths, the water surface follows the stream bed surface more closely than at shorter wavelengths. Thus, the hydrostatic damping factor for any arbitrary spatial wavelength or flow type can be evaluated using the following equation:

$$C_{damp}(Fr, \lambda)=\alpha(Fr)\ \beta(\lambda)\ C_{damp}(Fr_{ref}, \lambda_{ref}) \quad (16)$$

where the $\alpha(Fr)$ and $\beta(\lambda)$ (-) are the coefficients applied for variations in flow regime (-) and wavelengths (m), respectively; and the index *ref* represents the reference region displaying the observed data of Morén et al.'s (2017) field investigation (Paper I). Based on open channel theory, the ratio of the deviations of the water surface elevation to bedform elevation has a reverse correlation with the square of the Froude number under the steady-state condition:

$$\frac{dD_W}{dZ_B} = \frac{(dD_W/dx)}{(dZ_B/dx)} = \frac{1}{Fr^2-1} \quad (17)$$

where D_W (m) is the depth of surface water, and Z_B (m) is the bedform elevation. This calculation implies that a higher Froude number (i.e., the shift of the flow regime toward super-critical flow) leads to a shallower water depth compared with streambed surface fluctuation. Beyond this, assuming the direct relation between $C_{damp} \propto dD_W/dZ_B$ leads to the following equation:

$$\alpha(Fr) = \frac{C_{damp}(Fr,\lambda)}{C_{damp}(Fr_{ref},\lambda)} = \frac{Fr_{ref}^2-1}{Fr^2-1} \quad (18)$$

Furthermore, the data measured from a field investigation conducted by Morén et al. (2017) were used as the reference dataset to evaluate the hydrostatic damping factor in Paper I. The power spectra ratio is the square of the hydrostatic damping factor, as demonstrated below:

$$R_P = \frac{P_{WS}}{P_{BS}} = \frac{(A_{i,j})_{WS}^2}{(A_{i,j})_{BS}^2} = C_{damp}\left(Fr_{ref},\lambda_{ref}\right)^2 \quad (19)$$

where R_P (-) is the ratio of the power spectra of the stream water surface elevation, P_{WS} (m^2), to the streambed topography elevation, P_{BS} (m^2); A (m) is the amplitude of the rescaled fluctuation; and i and j are the wavelength numbers in x and y directions, respectively. Considering the Froude number given by Morén et al., (2017), the hydrostatic damping factor in Equation 17 can be represented as follows:

$$C_{damp}(Fr,\lambda) = \left(\frac{-0.9987}{Fr^2-1}\right)\left(\sqrt{R_P\left(Fr_{ref},\lambda_{ref}\right)}\right) \quad (20)$$

In Paper I, the power spectra ratio was fitted with an exponential function in which three additional exponential trends were considered as part of a sensitivity analysis (Figure 5).

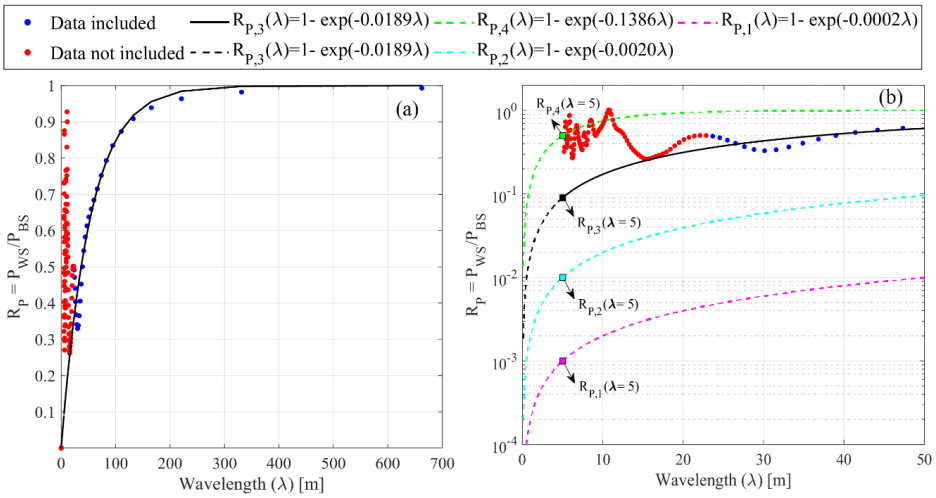

Figure 5. Ratio of water surface power spectrum to bedform power spectrum, $R_P = P_{WS}/P_{BS}$, used to estimate the hydrostatic damping factor in Paper I. Colored dots represent observed values from Morén et al. (2017), and the black line is the fitted value as a function of wavelength. (a) Fitted exponential function to the observed data; (b) Four exponential curves describing R_P, in which the dashed black line is the extrapolated exponential trend of R_P of the observed data as a function of wavelength. The colored, dashed lines are the three additional exponential curves representing R_P as functions of wavelength used to investigate the sensitivity of the hydrostatic head damping factor to the streambed-induced flow field.

On the other hand, the dynamic head component of the hyporheic flow fields resulted from the difference in the upstream and downstream flow velocities of the bedform. This component can be presented by introducing a dynamic head coefficient to the topography fluctuation (Elliott & Brooks, 1997a, 1997b). The dynamic head coefficient, which was previously expressed in Equation 11 (i.e., $\frac{h_m}{\sigma_{S,B}\sqrt{2}}$), is based on the standard deviation of fluctuation in the bedform evaluation, $\sigma_{S,B}$ (m), and the velocity head amplitude, h_m (m). The amplitude of the velocity head variation for a sinusoidal bedform shape is represented as follows (Fehlman, 1985):

$$h_m = 0.28\left(\frac{v_f^2}{2g}\right)\begin{cases}\left(\frac{Z_B/D_w}{0.34}\right)^{3/8} & Z_{BM}/D_w \le 0.34\\ \left(\frac{Z_B/D_w}{0.34}\right)^{3/2} & Z_{BM}/D_w \ge 0.34\end{cases} \quad (21)$$

where Z_B (m) is the height of the bedform variation and is estimated by $Z_B = 2\sqrt{2}\sigma_{S,B}$ (Stonedahl et al. 2010). The stream water velocity, v_f, and water depth of the stream channel, D_W, are quantified from directly measured values at the discharge stations (Figure 3) or estimated values using the proportion of the subcatchment area of the stream segments to the discharge stations' subcatchment area. The dynamic coefficient and hydrostatic damping factor spatially vary between the stream reaches within the catchment due to variations in streamflow velocity, flow depth, and Froude number.

3.3.2 Spatial representivity of hyporheic flow models

Due to the uncertainty in the hydrostatic head damping factor and dynamic head coefficient, various sensitivity analyses were conducted to provide an estimation of the degree of representivity of hyporheic flow models. Bedform topography variation, stream flow parameters (i.e., flow velocity and flow depth), the hydrostatic damping factor, and the depth of hyporheic zone were used in the applied sensitivity analyses to address the uncertainties in the hydrostatic and dynamic head contributions. Since the aim of these papers was to investigate the impacts of hyporheic fluxes and regional groundwater flow fields on each other; the hyporheic flow models had to be analyzed at many points of the watershed where the regional groundwater flow was evaluated. Finally, a combinatorial sampling on streamflow properties, topography realization, the hydrostatic damping factor, and the depth of the hyporheic zone was conducted as the applied sensitivity analysis in Paper I (Table 1). Next, Papers III and IV used Monte Carlo stochastic sampling to address the uncertainties in flow properties, topography realization, and the hydrostatic damping factor. Finally, details of the number of samples and description of each parameter in each scientific paper are described in Table 1.

Table 1. Schematic Description and Summary of the Considered Samples in the Sensitivity Analysis

Sensitivity Analysis Method		Flow Properties (Stream Flow Velocity and Depth)	Topography Realization	Hydrostatic Damping Factor	Hyporheic Depth
Paper I: Combinatorial Sampling Procedure	No. of Samples	14	20	4	2
	Description	Stream segments representing different stream orders	Selected from different parts of catchment	Evaluated from Morén et al. (2017) field measurement	Two different hyporheic depths (0.1 m and 4 m)
Paper III, Paper IV: Monte Carlo stochastic sampling (400 samples)	No. of Samples	30	20	400	-
	Description	Groups based on deep groundwater discharge points	Selected from different parts of catchment	Random number within 0–1 interval	Depth decaying hydraulic conductivity

3.4 Superpositioning of the Flow Fields

In this study, superimposing the groundwater flow fields with the hyporheic scale flow facilitated investigating the interaction between groundwater and hyporheic exchange fluxes. The individual flow fields for regional groundwater and hyporheic fluxes were evaluated separately and then superimposed on each other (Equation 12). Depending on the hypothesis of each paper, the superpositioning was conducted in either 2D (plains representing the streambed surface) or 3D (volumes containing the streambed sediment). Paper I focused on the impact of groundwater on the hyporheic flow field at the streambed interface. Hence, the groundwater flow velocities from different stream orders were extracted on a 2D surface (5×5 m^2 surface at the streambed interface; top surface of the 3D volume) from the streambed interface of the regional groundwater model. Next, these data were superimposed on the corresponding estimated hyporheic flow velocities at the topography surface. On the other hand, Papers III and IV focused on the impact of hyporheic fluxes on regional groundwater beneath the deep groundwater discharge locations at the topography surface. Consequently, the superpositioning was conducted in 3D domains, where the $5\times5\times5$ m^3 cubes were extracted from the deep groundwater discharge locations of the regional groundwater model and superimposed on the corresponding estimated hyporheic flow fields in $5\times5\times5$ m^3 domains. These superimposed models contained the flow velocities including both the regional groundwater and the hyporheic flow fields, facilitating the detailed study of convoluted nested flow process.

3.5 Statistical Analysis in Evaluation of Catchment Characteristic Parameters

Groundwater–surface water interaction across spatial and temporal scales depends on the subsurface properties that can influence the groundwater flow field. Hence, investigations of catchments' key independent (characteristic) parameters provided the required knowledge for generalization of subsurface flow results. Various catchment properties represented the following: local and regional landscape topography indexes (i.e., landscape elevation, e (m); standard deviation of landscape elevation, e_{std} (m); landscape topographical slope, S (-); gradient to closest stream, GtS (-); mean subcatchment size, MSC (m^2); standard deviation of elevation along the stream, Z-Str_{std} (m); elevation above the stream, EaS (m); area of the subcatchment, A_{sub} (m^2); distance to the catchment outlet, D_S (m); geological properties of the catchment (i.e., hydraulic conductivity of the soils, K (m/s), depth of the Quaternary deposits, Z_Q (m)); the

hydraulic properties of the streams (i.e., level, SW_a (m), and slope, SW_b (-)) of the spectral water density of the water surface profile; stream order, SO (-); stream water discharge, Q_{str} (m^3/s); the cross-sectional area of stream channel, A_{str} (m^2); the width of the stream channel, W_{str} (m); the depth of the stream water, D_W (m); the velocity of stream water, U_{str} (m/s); the slope of the stream channel, S_{str} (-); stream length, L_{str} (m); the stream flow Reynolds number, Re (-), the stream water Froude number, Fr (-); the Darcy–Weibach friction factor (-); and stream power, Str-P (N/s). All of these factors were used as independent (explanatory) variables during statistical analysis to determine the importance of those parameters for dependent groundwater and hyporheic flow velocities (Papers I, V). Additionally, Paper V used the averaged values of the independent parameters across three different scales: the reach scale, the intermediate subcatchment scale, and the regional catchment scale. The reach scale involved stream segments longer than 50 m without any tributaries, the intermediate subcatchment scales involved clustered adjacent subcatchments followed by the stream network, and the regional catchment scale involved the individual five considered catchments (Paper V). Principle component analysis (PCA) was used to identify the most essential explanatory parameters in a set of variables, and this operation was performed using a dimensional reduction method. Due to the large variation of the range of the considered parameters, the PCA was conducted on both raw data and the standardized datasets. Additionally, a multivariate power law regression model was used to find the correlation between the ratio of regional groundwater velocity over hyporheic exchange flow velocity and the independent catchment characteristic parameters:

$$\frac{W_C}{W_S} = \xi_1 C_1^{\xi_2} C_2^{\xi_3} \dots C_n^{\xi_{n+1}} \quad (22)$$

where W_C (m/s) and W_S (m/s) are the mean values of absolute vertical velocity of the regional and hyporheic scale models along the stream network, ξ (-) is the coefficient, and C refers to the independent characteristic parameters considered in the regression analysis. The performance of the model was evaluated by R^2, and adjusted R^2 (i.e., R^2_{adj}).

3.6 Field Investigation

The impact of various stream discharge intensities (i.e., representing different climatic conditions) on hyporheic exchange fluxes was studied through a field investigation during the summer of 2017 (7–24 of August; Paper II). The field investigation focused on a 1500-m stretch of the stream located between two discharge stations, namely C5 and C6, of the Krycklan catchment, where the C5 is located on the upstream side of Lake Stortjärn (Figures 3b and 6).

3.6.1. Field measurement

During the experiment, the stream water discharge was regulated by a gate at a V-notch weir located at Discharge Station C5. The weir's gate was completely closed for almost 3 weeks (7–24 of August) to simulate the low flow discharge intensity (representing the dry period) for the downstream side of the weir. Water pumped two times (August 19 and 21) into the experimental reach (from the upstream side at Station C5) to simulate high flow pulses. Details of the flow discharge intensities are provided in Table 2. Next, the stream water depth was measured every 50 meters along the stream segment on five different occasions to represent normal flow (May), summer base flow (August), low flow (during the experiment), and high flow (when the water was released twice from the weir's gate at the end of the experiment) conditions. Temperature was used as a natural trace element to assess the impacts of different flow discharges on surface water–groundwater interactions. Hence, the multi-level temperature sticks (MLTS) were installed at seven-point locations at the streambed interface along the stream network, representing both gaining and losing stream segments, as suggested by Leach et al. (2017). The temperature profiles were recorded at the following distances from the outlet of Lake Stortjärn toward Station C6: 150, 200, 350, 550, 620, 975, and 1100 m (Figure 6). The lengths of the temperature sticks were 66 cm (at 150, 200, 350, 550, 620, 1100 m) and 105 cm (at 975 m). The temperature was recorded

at -60, -35, -25, -20, -15, -10, -5, and 0 cm from the head for the short sticks (i.e., 66 cm length), whereas the depths of the sensors were at -83, -65, -48, -31, -23, -17, -13, and 0 cm from the head of the lance for the long stick (105-cm temperature stick located at 975 m). The temperature was recorded at a 5-min temporal resolution throughout the entire experimental period.

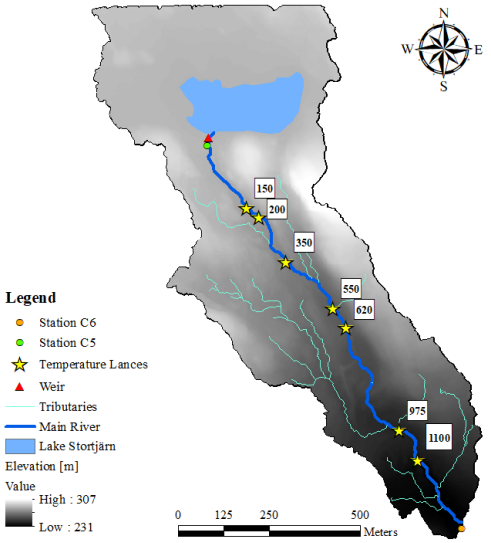

Figure 6. Map showing the field investigation subcatchment and its topography and Lake Stortjärn, the main river within the subcatchment, and its tributaries. Additionally, the upstream (C5) and downstream (C6) discharge stations are shown. The location of the V-notch weir and temperature lances are also presented.

Table 2. Details of the Flow Discharges of the Stream Stretch During the Field Investigation

Flow Discharge	Time Period	Mean Upstream Discharge [L/s]	Mean Downstream Discharge [L/s]
Base flow	03–07Aug.	8.71	10.8
Low flow	07–19 Aug.	0.22	1.56
High flow 1	19 Aug. (07:22 until 18:17)	25.59	27.96
High flow 2	21 Aug. (06:15 until 09:07)	25.57	30.09

3.6.2. Flow modeling of the field investigation

A two-dimensional numerical model of longitudinal transect along the main stream network of the field study area was developed using COMSOL Multiphysics® software. The stream morphology was represented with a 50-cm resolution DEM file. The bedrock surface elevation with 10 m resolution (©Sveriges geologiska undersökning, SGU) was used in the numerical model. Next, two different scenarios of streambed sediment hydraulic conductivity were analyzed regarding surface water–groundwater interaction. This analysis used the following elements: (a) a constant hydraulic conductivity of 10^{-4} (m/s) for the entire subsurface domain (i.e., streambed sediment and Quaternary deposits); (b) a depth-decaying hydraulic conductivity based on Equation 14 for the top meter of the subsurface region (i.e., representing streambed sediment),

beginning with the hydraulic conductivity of 10^{-4} (m/s) at the sediment–water interface and decaying to 10^{-7} (m/s) at the depth of 1 m; and the rest of the Quaternary deposit (deeper than 1 m from the topography) assumed to have a hydraulic conductivity of 10^{-7} (m^2), representing the glacial sediment soil type of the Krycklan catchment (Sterte et al., 2018). Individual models were developed for each of the flow discharge intensities where the steady-state condition was applied for the subsurface flow modeling. The measured water level values of the discrete observational points (each 50-m interval) were linearly interpolated (at 0.5 m resolution) along the main river network during different discharge intensities. The interpolated water level reflecting hydrostatic hydraulic head was used as the top boundary condition of the numerical models. Consequently, the role of the dynamic hydraulic head due to additional pressure induced by streamflow velocity over the bedform was neglected in Paper II. Furthermore, the fixed head boundary condition was used for both the upstream and downstream sides of the model, but no flow boundary condition was applied on the bottom surface. A particle tracing routine was applied by releasing 1,000 uniformly spaced inert particles distributed across the streambed sediment to evaluate the impacts of discharge intensity on hyporheic flow residence time and depth of hyporheic zone. In this study, the residence time of hyporheic flow, τ (s), was defined as the time taken by the hyporheic water to flow from the recharge at the streambed interface into the subsurface domain until returning to the streambed interface again.

3.7 Particle Tracing in the Hyporheic Zone

Changes in direction and travel time of groundwater flow near the streambed surface due to the impact of hyporheic fluxes were the main parameters investigated to deduce the impact of hyporheic exchanges' fluxes on groundwater flow fields (Paper III, IV). The extracted 5×5×5 m^3 cubes from the regional groundwater model contained both intermediate groundwater and deep groundwater flow. In this context, intermediate groundwater flow is the groundwater flow field that has never been in the bedrock layer, and its entire flow path is confined to the Quaternary deposit and streambed sediments (Figure 7). The particle tracing in the hyporheic zone was conducted by releasing particles at inflow points along the streambed using a grid of 50×50 inert particles uniformly distributed at the bottom surface of the 5×5×5 m^3 cubes. However, these particles represent only the intermediate and deep groundwater flows in superimposed 5×5×5 m^3 cubes. Next, the particles were tracked within the streambed domain until reaching the top surface or leaving the cubes from the lateral surfaces. The impact of hyporheic fluxes in nested flow systems near the streambed surface was investigated using the variation of travel time of each individually released particles in both the absence and presence of hyporheic flows.

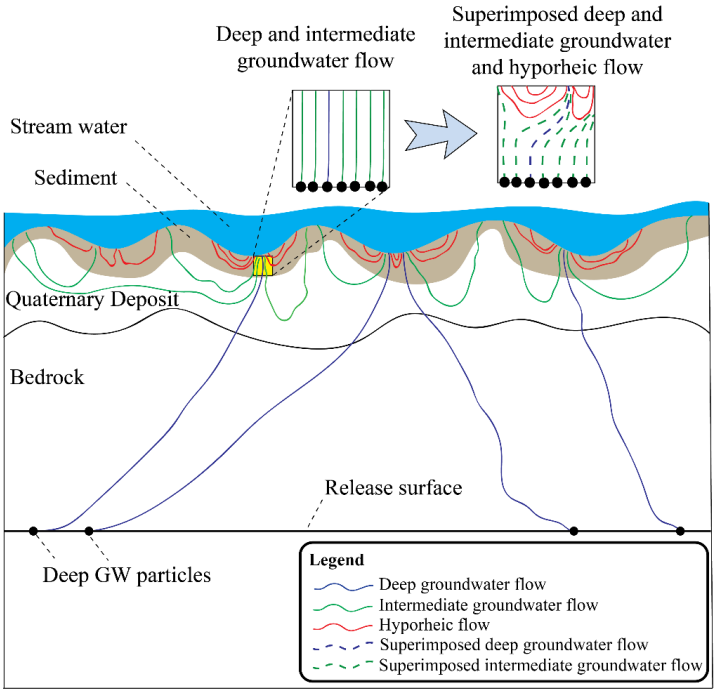

Figure 7. Schematic cross-sectional sketch showing the multiscale flow processes considered in the present study. The catchment-scale model covers only the deep and intermediate groundwater flow fields (blue and green solid lines), whereas the streambed-scale model evaluates the hyporheic fluxes (red solid lines). The superimposed deep and intermediate flows (blue and green dashed lines) are influenced by hyporheic fluxes.

3.8 Fragmentation of Coherent Discharge and Recharge Areas

The surface water–groundwater interaction in a hyporheic zone influences the recharge and discharge areas of both of these water types at the stream water interface. Additionally, the spatial distribution of regions with gaining or losing conditions at the streambed interface was investigated during this PhD study (Papers I, II, III, and IV). The gaining condition was defined as discharge areas at the streambed interface containing only upwelling flow, whereas the losing condition occurred in the regions with only downwelling fluxes. The fragmentation analysis was performed on an orthogonal mesh with the spatial resolution of 0.1×0.1 m^2, where the exchange velocity at the streambed interface was taken in an orthogonal direction (not in diagonal directions). Coherent areas with flow in only the upward or downward direction were represented by a cumulative distribution function (CDF), in which the frequencies of the sizes of spatially coherent areas were weighted by their areas (i.e. area percentage). Fragmentation of coherent exchange flow areas is the distribution of coherent upwelling or downwelling areas, where increasing fragmentation referred to a shift in the CDF toward smaller areas. Additionally, the fragmentation of hyporheic fluxes at the streambed interface under the influence of regional groundwater flow was investigated in Papers I and II. At the same time, the fragmentation of coherent upwelling areas containing the deep groundwater flow along the streambed topography was studied in Papers III and IV.

4 RESULTS AND DISCUSSION

In this section, the most important results of this thesis project are presented. This project produced the five attached papers, which investigate the complexity of surface water–groundwater interaction occurring within streambed sediment. This study followed the applied methods in evaluating the regional and hyporheic flow fields, separated by utilizing the numerical model, exact solution, and the field investigation. The results presented in each section are followed by a brief discussion; however, detailed discussions are found in the discussion section of the appended papers.

4.1 Representing Groundwater Elevation with Landscape Topography

Landscape topography elevation is often used as the top boundary condition in terms of the hydraulic head for the regional scale groundwater flow modeling. This condition is a simplified reflection of the fact that the groundwater surface elevation is often a subdued, smoothed replica of the landscape topography. This assumption is valid for a region with a humid climate and shallow soil depth, containing bedrock with low permeability properties. However, the natural boundary conditions can be exactly represented by applying landscape topography elevation for the landscape regions where surface water exists (the Dirichlet boundary condition), whereas infiltration prevails for the rest of the terrain (the Neumann boundary condition). Over infiltration regions, the groundwater table is smooth and subdued compared with the landscape topography, aspects that can be represented by reducing the resolution of the landscape DEM before being applied as representations of the ground water table. Previous research has illustrated the impact of the DEM resolution on modeled groundwater flow fields, when increasing the DEM mesh size leads to a lower modeled groundwater exchange velocity at the top boundary, meaning lower infiltration (Marklund & Wörman, 2011; Wang et al., 2018). In Paper IV, we successfully decreased the DEM resolution only over the recharge zones through an iteration process so that the recharge rate corresponded to the infiltration estimated independently from the data. The mean value of regional absolute vertical velocity at the top surface, $\langle |W_C| \rangle$, was used to highlight the difference between application of original DEM resolution and the revised variable DEM resolution on modeled groundwater flow. The results indicated that using the 2-m resolution of the DEM file (the resolution of the original DEM dataset) for the entire topography surface of the Krycklan catchment led to a 3,073 mm/year groundwater flux at the topography surface. At the same time, decreasing the DEM resolution to 70-m, 84-m, and 120-m resolutions of only recharge areas substantially decreased the groundwater flux at the topography surface to 542 mm/year, 379 mm/year, and 203 mm/year, respectively (Figure 8). The groundwater flow velocity at the water table (z=0) resulted from the Krycklan topographical DEM file with resolution of 84-m (over the downwelling zones), and 2 m (over the upwelling zones) was approximately equal to the annual mean run off value from the precipitation rate (382 mm/year); and thus, it was kept as the plausible DEM file for modelling set up (Paper IV). Application of the variable DEM resolution file as the input for the regional groundwater model made it possible to satisfy the natural boundary condition of both the Dirichlet (i.e., topography-controlled head at lakes and streams) and the Neumann (i.e., recharge-controlled head at terrain with downward flow direction) boundary conditions in a single model.

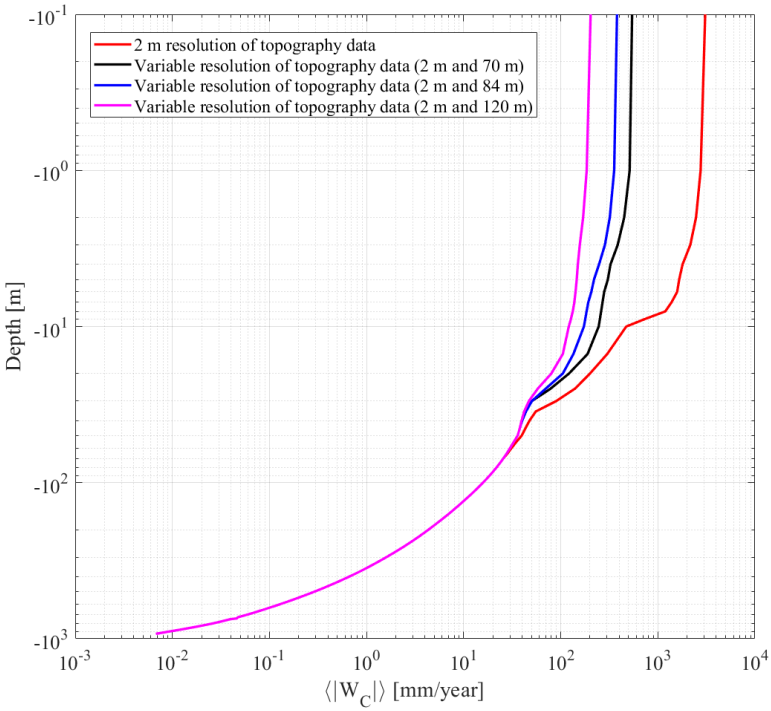

Figure 8. Mean values of the absolute vertical velocity of the catchment-scale model, $\langle|W_C|\rangle$, in depth. The results concern the value of $\langle|W_C|\rangle$ using a 2-m resolution DEM (red line) and a variable-resolution DEM with 2 m (at upwelling regions) and 70 m (at downwelling regions) (black line); 2 m (at upwelling regions) and 84 m (at downwelling regions) (blue line); and 2 m (at upwelling regions) and 120 m (at downwelling regions) (magenta line) (Paper IV).

4.2 Regional Groundwater Flow Results

Analyzing the results of the regional groundwater flow model facilitates understanding of the fate and transport of solutes and contamination carried by groundwater flow from different spatial scales, including deep and intermediate convoluted flow fields (Carucci et al., 2012). In particular, the study examined the fate and transport of hypothetical radiological contaminants leaking from an HLRW and carried by deep groundwater flow. This analysis involved releasing 10,000 uniformly distributed particles located at a depth of 500-m (Paper IV). Additionally, the distribution of travel times (evaluated by seepage velocity) of the deep groundwater fluxes was presented for different subsurface layers (i.e., bedrock, Quaternary deposits, and streambed sediment). The results indicated substantial variations in the travel times of inert particles (representing deep groundwater fluxes) released at 500-m depth in different layers, where the median travel times in bedrock, QD, and streambed sediments were 750, 10, and 8 years, respectively (Figure 9). These variations arose from different porosities, hydraulic conductivity values, layer thicknesses, and variations in groundwater flux intensity reaching the subsurface layers. The travel times for deep groundwater flow in QD and streambed sediment are approximately in the same order, whereas the travel times for flow in the bedrock domain are one to three orders of magnitude greater. However, including the retardation of solutes due to the adsorption process can significantly increase the solutes' transport time in subsurface strata, especially in Quaternary deposits and sediment layers. In particular, the transport time of ^{135}Cs

were found to be in the same order of magnitude, about 1,000 years, within all of the subsurface domains (bedrock, QD, and sediment). These results could highlight the importance of QD and streambed sediment in safety assessment programs compared to those of the bedrock domain, where radionuclide transport is more prolonged in aquatic sediments than in the bedrock domain. Consequently, the retardation and prolonged transport times of radionuclide compounds in the shallow subsurface domain may prolong and increase the exposure of agricultural products and aquatic habitats (Avila et al., 2013; Torudd & Saetre, 2013). Therefore, despite the shorter travel time of the radionuclide transport in streambed sediments for inert solutes compared with the spent time in bedrock and Quaternary deposits, the greater retardation of radionuclides increases the risk of radiological doses to humans and other living biotas. The latter condition makes the aquatic sediments a unique environment that should be investigated in detail in the safety assessment of certain leakage scenarios from the HLRW.

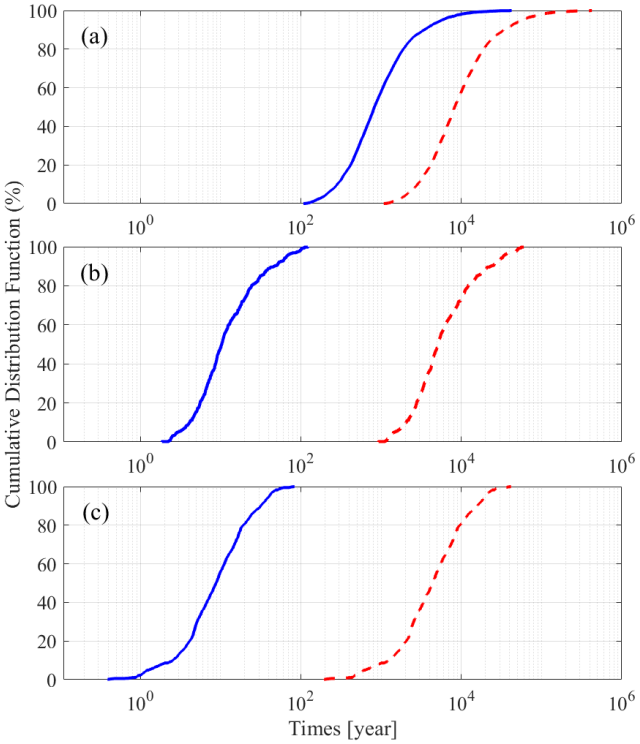

Figure 9. Cumulative distribution function plot of the water travel time (solid blue line) and ^{135}Cs transport time (dashed red line) in (a) bedrock, (b) Quaternary deposits, and (c) sediment domains. These results correspond to the particles with initial positive vertical velocities, which were released from a depth of 500 m from the minimum topography elevation and reached the top surface (Paper IV).

The discharge locations of deep groundwater flow at the topography surface follow the location of surface water objects, especially the stream network (Marklund et al., 2008). In this study, the results of the regional scale model's particle tracing revealed that almost half of the particles released at a depth of 500 m (i.e., 4434 particles) represented the upward deep groundwater flow (with positive vertical velocity at their initial positions). In this flow, 2,743 particles eventually reached the topography surface of the watershed model domain (Paper IV). Figure 10 displays the discharge locations of the deep groundwater flow at the topography surface (which were

evaluated using the aforementioned particle tracing approach). In these areas, 1,552 discharge points were located within the catchment boundary, and 1,191 reached the topography surface outside of the Krycklan catchment boundary (Paper IV). The majority of discharge points aligned as well as expected with the stream network (approximately 90% of the discharge points) and lakes (approximately 10% of the discharge points), reflecting the role of local topography elevation gradient in subsurface flow circulation. The clustering of the discharge points along the stream network and lakes was due to the fractality of the topography surface and the hierarchic nature of the groundwater flow cells, demonstrating a controlling effect on the regional groundwater circulation (Wörman et al., 2007; Marklund & Wörman, 2011). Additionally, convergence of the deep groundwater discharge toward the surface of the landscape demonstrated a reduction in the area contaminated by radionuclides that could leak from an HLRW in the future. Notably, most of the discharge points are found in the downstream region of the catchment, where the topography is relatively flat, containing soil with higher hydraulic conductivity and a deeper Quaternary deposit compared with the upstream regions of the catchment. Similar conditions were found by Marklund et al., (2008) and Caruso et al., (2016).

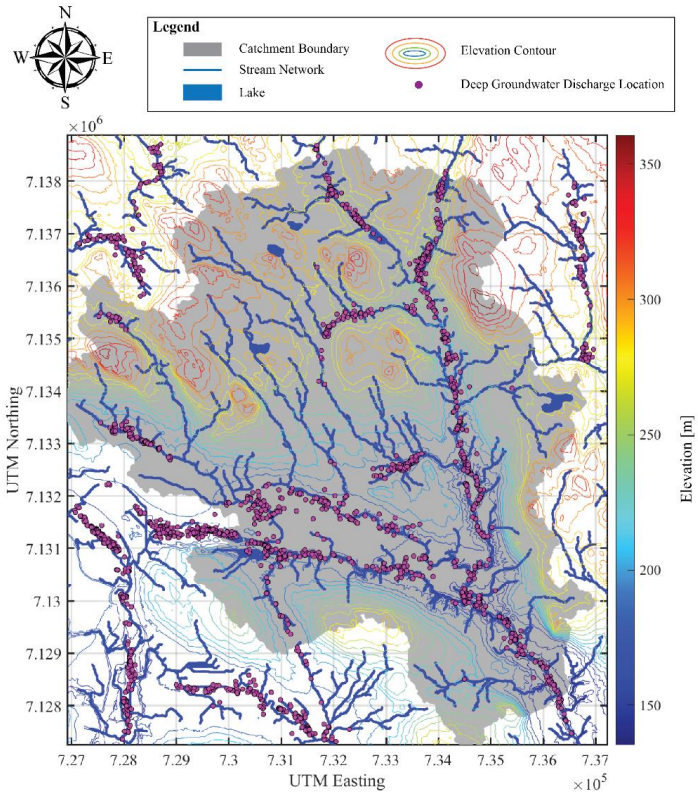

Figure 10. Discharge locations of the particles released from a depth of 500 m from the minimum topography elevation of the catchment. The discharge locations are represented by purple points. Additionally, the topography elevation range is presented with contours in which colors range from blue to red as the elevation increases. The stream network and the catchment boundary are represented by the blue line and gray zone, respectively (Paper IV).

The regional groundwater flow along the stream network contains both upward and downward flow directions but predominantly upward because the stream system facilitates drainage of the watershed. The absolute value of the groundwater flow velocity expresses the magnitude of the water flux regardless of its direction. Beyond this, the topography variation and the heterogeneity of hydraulic conductivity of the subsurface domain impact the magnitude of the groundwater flow at the streambed interface (Conant, 2004; Rinderer et al., 2014). Thus, the study used stream order to represent location variation in the catchment from upstream to downstream. For this reason, variation of subsurface soil type was used as the criterion by which to study the magnitude of groundwater flow at the stream water interface (Paper I). Furthermore, areal mean value (based on 5×5 m^2 regions surrounding the stream network) of absolute vertical exchange velocity at the groundwater-surface water interface, $\overline{|W_C|}$, was evaluated for different stream orders (i.e, first, second, third, fifth) to highlight the variability of the groundwater recharge and discharge within the catchment. First-order streams located in headwaters reflects relatively higher elevation compare to other stream orders; whereas fifth-order streams located downstream part of the catchment close to outlet in which the region has relatively flat topography surface and deep Quaternary deposits (refer to Paper I for the location of selected stream orders). As shown in Figure 11, the groundwater exchange fluxes have higher intensity in first-order streams than in other stream orders. The results showed no clear difference between the second, third, and fifth stream orders, whereas there was a considerable difference in the range of their interquartile. This result was due to the number of selected stream segments for each stream order. For instance, only one stream segment was selected for the fifth stream order (there was only one fifth-order stream accessible at the study site). In addition, the shorter interquartile range indicated a larger homogeneity of factors controlling groundwater flow in first- and fifth-order regions of the study site.

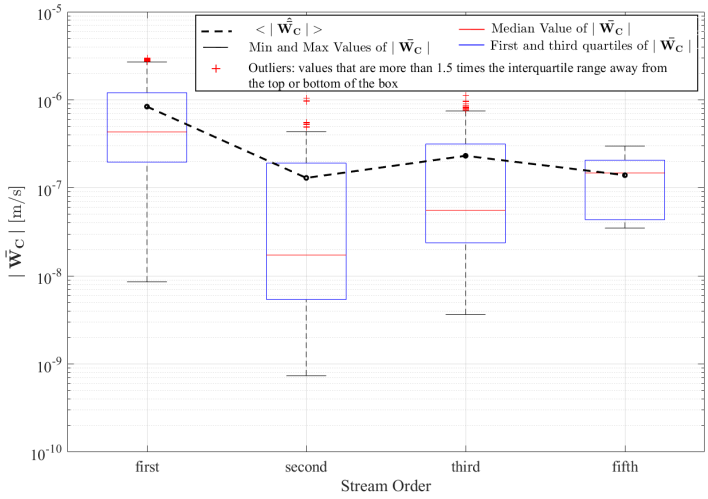

Figure 11. Box and whisker plot of the absolute values of the areal mean values of the vertical component of catchment-scale groundwater velocities at the streambed interface $\overline{|W_C|}$ in 5×5 m^2 areas characterized by different stream orders

4.3 Hyporheic Flow Results

Hydrostatic and dynamic head contributions to the total hyporheic hydraulic head along the streambed interface control the magnitude of the hyporheic flow field. Previous studies have highlighted the importance of Froude number and streambed topography fluctuation in evaluating the hydrostatic and dynamic head components of the hyporheic head (Tonina &

Buffington, 2007; Käser et al., 2013). In this study, the fractal nature of the bed topography fluctuation (Jerolmack & Mohrig, 2005; Nikora et al., 1997; Wörman et al., 2007) allowed generalization of streambed topography to a wide range of spatial scales for the evaluation of hyporheic flow. Therefore, a rescaled topography was used to represent streambed topography and to separately define the hydrostatic and dynamic head contributions. This goal was accomplished by introducing a hydrostatic damping factor and a dynamic head coefficient (Section 3.3.1). Additionally, the depth of the hyporheic zone (i.e., depth to the "no-flow" boundary in hyporheic flow modeling used in Paper I) controls the magnitude of hyporheic exchange flow velocity and thus the flow residence time in streambed sediment (Morén et al., 2017). Hence, two different sampling approaches, deterministic-combinatorial (Paper I) and stochastic Monte Carlo (Paper III, IV) samplings, were used for different parameters included in sensitivity analysis to cover the existing uncertainties in the hydrostatic and hydrodynamic components of total hyporheic hydraulic head (Table 1). The results of the combinatorial sampling analysis on 18 stream segments (representing first, second, third, and fifth stream orders) expressed with the areal mean value of absolute hyporheic vertical flow velocity, $\overline{|W_S|}$, highlighted the predominant role of the hydrostatic damping factor compared to the dynamic head coefficient on the magnitude of total hyporheic hydraulic head (Paper I). In addition, considering a fixed, no-flow boundary at shallow depths in hyporheic modeling (refer to the depth of hyporheic fluxes in Paper I) increased the impacts of local bedform variation; an impact represented as "shielding effect" plays a crucial role on the hyporheic flow components, especially since it changes the magnitudes of hydrostatic and dynamic flow components up to a single order of magnitude (Figure 12). The role of dynamic flow contribution was more evident in first-order streams representing the headwaters where the Froude number was higher than in the rest of the stream orders. Furthermore, the shallower hyporheic zone resulted in an increased shielding effect, leading to higher magnitudes of hydrostatic and dynamic head components and hence higher hyporheic exchange fluxes.

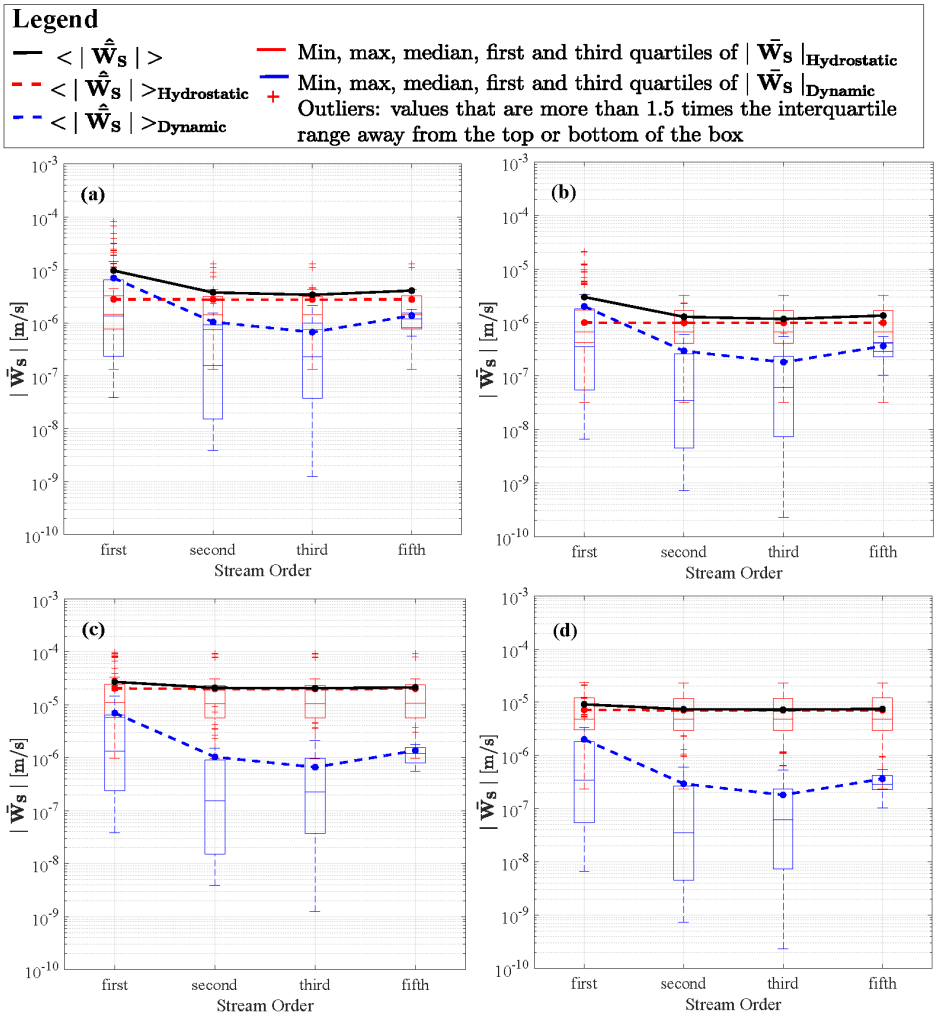

Figure 12. Box and whisker plots of the areal mean values of the vertical components of streambed-scale-induced flow velocities in 5×5 m^2 areas from different stream orders assuming four different scenarios of the damping of the surface water fluctuations and depth of the hyporheic zone: (a) $R_{P,2}$ and ε=0.1 m; (b) $R_{P,2}$ and ε=4 m; (c) $R_{P,4}$ and ε=0.1 m; (d) $R_{P,4}$ and ε=4 m (Paper I)

The impact of hyporheic fluxes on deep upwelling groundwater within the streambed sediment can significantly affect the retardation of radionuclide compounds that are leaking from the deep waste repository and discharge with deep groundwater flow in aquatic sediments. In turn, this process affects the risk of radiological doses' entering humans and other living biotas. Papers III and IV used a Monte Carlo sampling method to explore the uncertainty in hydrostatic and dynamic head coefficients at the deep groundwater discharge zones. The method used 400 randomized combinations of hydrostatic damping factor (from a uniform distribution in the range of [0–1]) and streambed topography (from 20 arbitrary realizations of the bedforms) for stream segments identified in 30 different subcatchments (representing streamflow properties

such as flow velocity and flow depth). The results highlighted the role of the Froude number of the stream flow for the dynamic head; whereby higher Froude number led to a relatively increased contribution of the dynamic head (Figure 13). Additionally, the results presented in Paper IV indicated that the hydrostatic head component dominated the total hyporheic hydraulic head for Froude numbers less than 0.45. However, most of the applied stream flow properties in Paper IV were associated with a Froude number less than 0.45. All of the results from this project demonstrated that the hyporheic flow field always had a mean value in the range of 10^{-6}–10^{-5} (m/s) at the streambed. Furthermore, these results indicated that hydrostatic head contribution has a more significant role than dynamic head contribution in the total hyporheic hydraulic head, a fact neglected in previous studies (Caruso et al., 2016; Marzadri et al., 2014). This neglect has led to underestimation of the hyporheic flow field and may result in a lower hyporheic flow contribution to upwelling subsurface discharge flow at the streambed interface compared with that of the regional groundwater flow contribution.

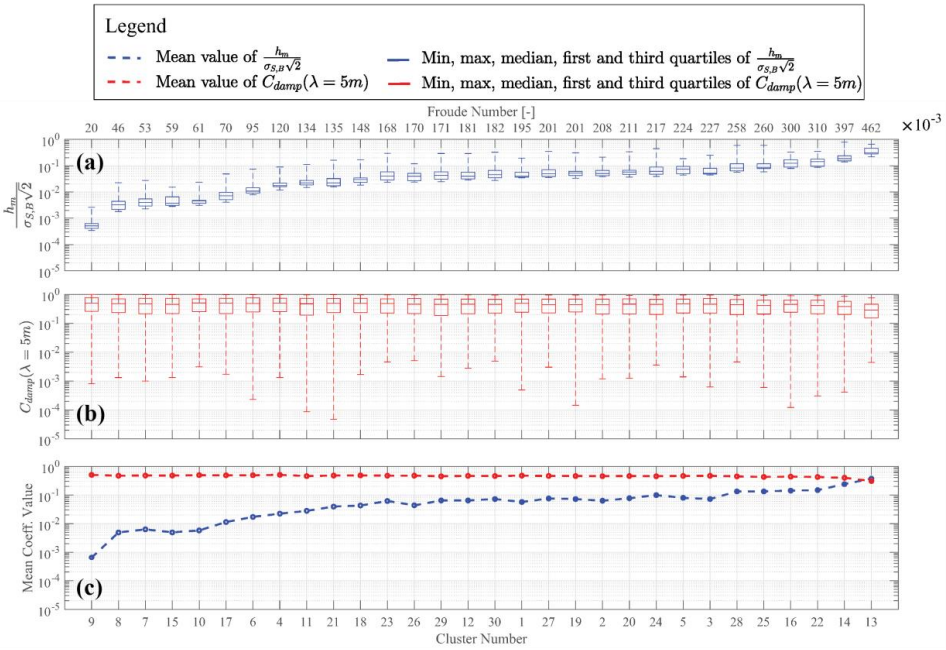

Figure 13. Streambed-induced hydraulic head factors that were used in the Monte Carlo simulation for different areas in different parts of the study catchment sorted by Froude number: (a) distribution of the dynamic factor for each drainage area, (b) distribution of the hydrostatic damping factor for each drainage area, (c) mean value of dynamic coefficient (blue color) and hydrostatic damping factor (red color) for each drainage area

4.4 Groundwater–Surface Water Interaction

The groundwater–surface water interaction occurring within the hyporheic zone was investigated from two different perspectives. These were (a) the influences of groundwater flow on hyporheic fluxes (Paper I) and (b) the impacts of hyporheic flow on the upwelling groundwater discharge zones (Paper III, IV). One implication of groundwater–surface water interaction is the change in both surface water and groundwater flow residence times within the hyporheic zone, affecting the diversity of aquatic habitat and the quality of the surface water (Poole et al., 2006). Additionally, the heat and solute transported via groundwater impact the hyporheic exchange

flow quality (Bhaskar et al., 2012). In general, the regional groundwater influences the depth of hyporheic zone, whereas the hyporheic exchange flow field influences the upwelling groundwater velocity and direction (Cardenas & Wilson, 2006; Boano et al., 2009). During this study, the impacts of different topographical scales for the subsurface flow were investigated by applying superpositioning of different scale intervals based on Equation 12. This process was motivated by the linearity of Equation 8. The changes in flow velocity, flow direction, flow travel time, and the sizes of discharge zones were investigated in this study to reflect the importance of topography in the hierarchically nested flow structure. Previous investigations have considered only the dynamic head contribution of the hyporheic hydraulic head in interactions between surface water and groundwater (Caruso et al., 2016; Marzadri et al., 2014). However, these results highlighted the major role of the hydrostatic head in the total hyporheic flow field. Neglecting this impact could lead to exaggeration of the importance of groundwater flow contribution in the nested flow system at the streambed interface.

4.4.1 Flow velocity: Groundwater flow and hyporheic exchange fluxes

The impact of groundwater flow on hyporheic flow velocity was evaluated through comparisons between contributions of hyporheic exchange fluxes and groundwater flow in total subsurface nested flow velocity at the streambed interface for different stream orders. The results in Paper I indicated that the mean values of absolute vertical velocity (averaged over stream order) of the hyporheic fluxes, $\widehat{|W_S|}$, were always greater than the mean values of absolute vertical velocity of regional groundwater, $\widehat{|W_C|}$, at the streambed interface, regardless of the assumed hydrostatic damping factor and stream flow properties (Figure 14). However, increasing the hydrostatic damping led to increased suppression of the hyporheic flow velocity and, consequently, the larger contribution of the groundwater flow in total subsurface nested flow velocity. The hydrostatic damping factor was hypothesized to be a function of topographical wavelength and stream flow Froude number. However, the effect of Froude number on hydrostatic damping factor was found to be relatively small compared with the impact of topographical wavelengths of the streambed. Furthermore, increasing the depth of the hyporheic zone lowered the magnitude of hyporheic flow velocity and increased the contribution of groundwater flow to average subsurface nested flow velocity at the streambed interface. Since flow travel time and flow velocity are inversely proportional, the decreased hyporheic flow velocity due to the increased hyporheic depth resulted in prolonged travel times for hyporheic flow. This result confirms the findings of Morén et al. (2017) regarding the fact that increasing hyporheic depth leads to an increase in hyporheic travel time within streambed sediment. Beyond this, the magnitude of the hyporheic fluxes controls the gaining and losing segments at the streambed interface (Fox et al., 2014), and the increased magnitude of hyporheic exchange vertical velocity can potentially enhance the stream denitrification in large stream basins (Gomez-Velez et al., 2015).

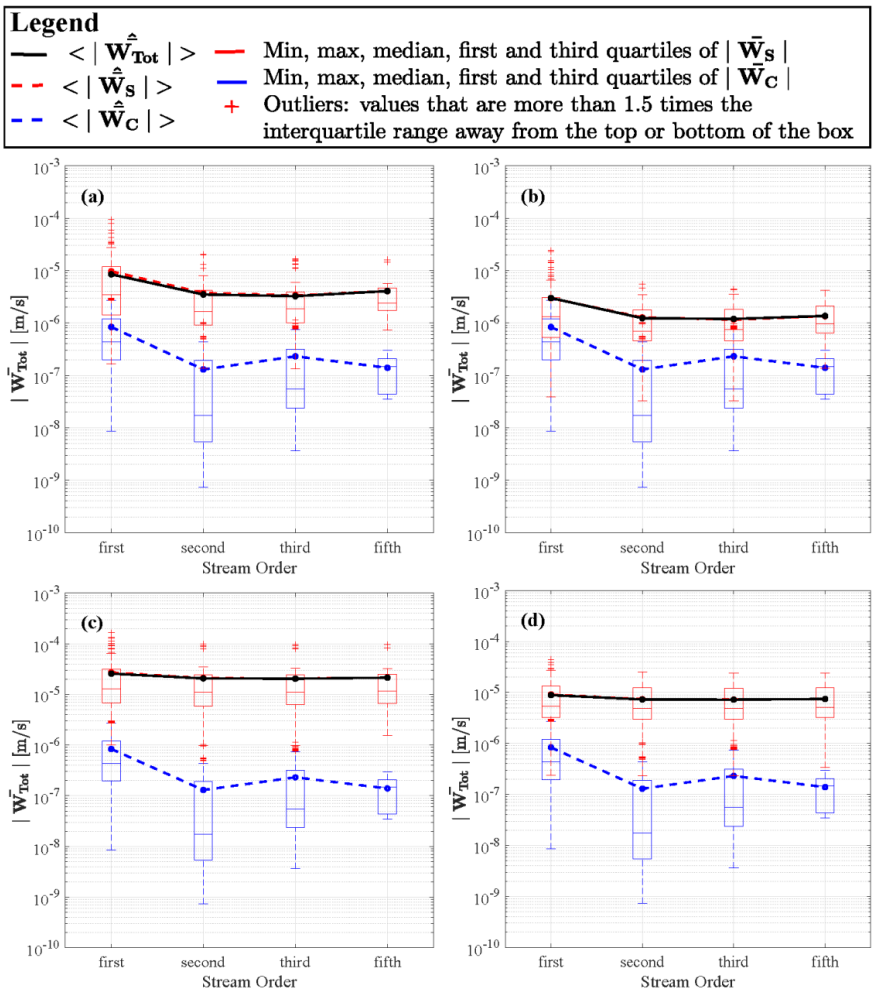

Figure 14. Box and whisker plots of the superimposed means of the areal mean values of the absolute vertical velocity in 5×5 m² areas from different stream orders assuming the following: (a) $R_{P,2}$ and ε=0.1 m; (b) $R_{P,2}$ and ε=4 m; (c) $R_{P,4}$ and ε=0.1 m; and (d) $R_{P,4}$ and ε=4 m.

4.4.2 Impact of hyporheic fluxes on groundwater travel time in streambed sediment

In this study, particle tracing in streambed sediment was conducted to quantify the groundwater flow travel time in streambed sediments (refer to Section 3.7). The results demonstrated that the subsurface groundwater flow travel time within the streambed sediment depends on the penetration depth of the groundwater flow. Additionally, shallower groundwater flow has a shorter flow travel time within the streambed sediment (Paper IV). In particular, it was demonstrated that the median travel times (related to the seepage velocity) of the intermediate groundwater that never entered the bedrock and deep groundwater flow coming from a 500-m depth were 3 and 9 years in streambed sediment, respectively (Figure 15). The decreased travel time of groundwater flow (originating from different spatial scales) within the same layer (i.e., streambed sediment) reflected the relatively lower flow velocity of intermediate groundwater flow compared with deep groundwater flow in streambed sediment. Superimposing the hyporheic

flow field on the intermediate and deep groundwater flows in streambed sediment led to the acceleration of the regional groundwater discharge through the hyporheic zone and thus decreased the travel time of both intermediate and deep groundwater flows. These results indicated that the travel time of subsurface flow decreased by a factor of almost 3. The deep and intermediate fluxes' travel times in streambed sediment were 3 and 1 years, respectively, under the impact of hyporheic flow fields. The intermediate flow travel time was approximately one-third of the deep groundwater travel time (within the streambed sediment), regardless of the presence or absence of hyporheic flow fields. Additionally, the results showed that the hyporheic flow field had a stronger impact on longer travel times of subsurface groundwater flow (both intermediate and deep flows). One implication of these results is a significant impact of the hyporheic zone on the fate and transport of solutes and contaminants carried by groundwater from different depths. Furthermore, changes in the travel time of the groundwater flow induced by hyporheic fluxes near the bed surface impact the diversity in aquatic sediment habitat and influence stream water quality (Poole et al., 2006). In particular, the residence time of the leaked radionuclide contamination from a deep repository carried by deep groundwater was affected by the hyporheic fluxes near the bed surface. Finally, the decreased groundwater travel time in streambed sediment would result in higher rate coefficients in the compartment modeling of radionuclide transport in the surface environment (Xu et al., 2008).

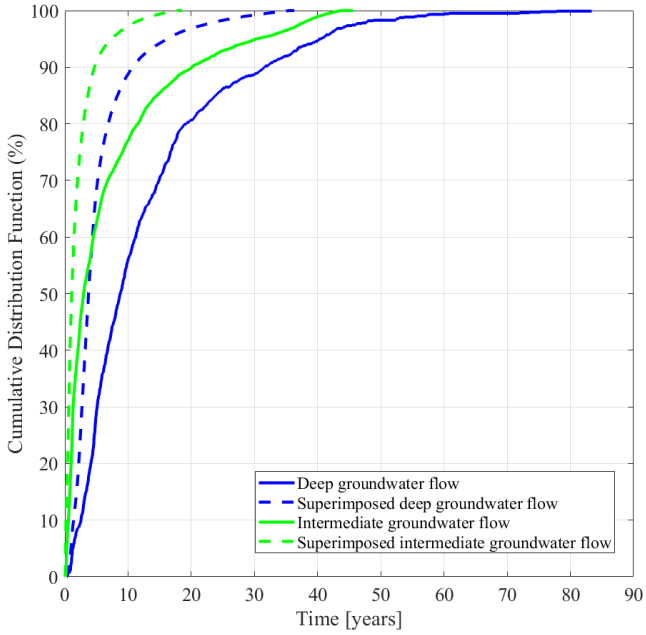

Figure 15. Cumulative distribution function plot of the intermediate (green) and deep (blue) travel times (using seepage velocity) of the groundwater flow within the sediment layer (i.e., 5×5×5 m^3 cubes). The solid lines represent the catchment scale results (without the streambed induced flow influence), and the dashed lines represent the superimposed results (catchment scale flow superimposed with the streambed scale induced flux). Descriptions of the different flow types are presented in Figure 2.

4.4.3 Convergence of groundwater flow field due to hyporheic fluxes' impact within streambed sediment

This project investigated the impact of hyporheic fluxes on the direction of upwelling groundwater flow beneath the deep groundwater discharge zones (Papers III and IV). The results

revealed that the subsurface groundwater upward flow (induced by different topographical scales) in streambed sediment was significantly influenced by the hyporheic fluxes, leading to the convergence of groundwater flow trajectories near the bed surface. This convergence is consistent with the hierarchical structure of flow cells, which accelerates the flow toward the top surface of the flow domain (Toth, 1963) but in this study was especially pronounced exactly at the discharge zones. Consequently, the upward groundwater flow shrank into small areas penetrating the hyporheic zone within the aquatic sediments. The impact of hyporheic fluxes on upward groundwater flow direction were previously investigated by Boano et al., (2009). However, the focus of their research was on the suppression of hyporheic exchange fluxes due at the groundwater upwelling zones. The convergence of the upward groundwater flow toward the streambed shows the diversity in temperature and chemistry of the hyporheic zone (Mamer & Lowry, 2013). The depth where the hyporheic fluxes begin to significantly impact the direction of upward groundwater (i.e., the depth at which the convergence of upward groundwater flow begins) depends on the hydraulic conductivity of streambed sediment and the magnitudes of hyporheic and groundwater flow velocities. In particular, the spatial heterogeneity of streambed sediment influences the direction and magnitude of the hyporheic flow field (Sawyer & Cardenas, 2009; Jiang et al., 2011). Applying a constant hydraulic conductivity throughout the entire streambed sediment depth (5 m) made a significant impact on upward groundwater flow induced by hyporheic fluxes (Paper III). Additionally, the results of assuming a constant hydraulic conductivity of streambed sediment (with a fixed depth of streambed sediment layer) demonstrated that the upward groundwater flow converged toward the topography surface (due to the impact of hyporheic exchange fluxes) as soon as it passed the bottom surface of the streambed sediment layer (Figure 16).

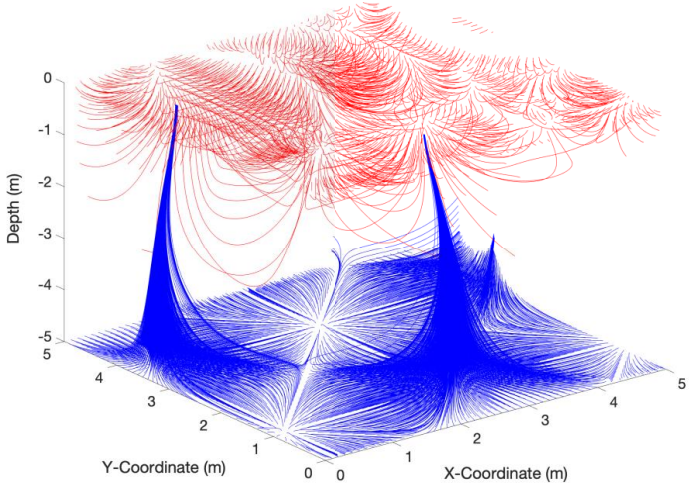

Figure 16. Three-dimensional plot of the interaction of local (hyporheic) flow (red curves) and regional upwelling groundwater (blue curves). The particle tracking of the hyporheic flow (red curves) was performed by releasing particles at inflow areas of the surface water on the top surface. The upwelling groundwater was tracked by releasing particles uniformly at the bottom surface.

However, applying a depth-decaying hydraulic conductivity function according to certain observations (Paper IV) changed the hyporheic flow depth. The depth-decaying hydraulic conductivity controlled the hyporheic fluxes' penetration depth and allowed the upwelling groundwater to stay in its trajectory even in streambed sediment (until reaching the hyporheic fluxes). The results of applying depth-decaying hydraulic conductivity in streambed sediments

showed that the convergence in upward groundwater gradually begins in the range of 2–3 m from the streambed topography surface (Figure 17). The upward groundwater flow was fragmented into a few detached flow tubes, which eventually emerged as the small areas at the streambed interface. Figure 17a.b shows a stronger impact of hyporheic fluxes on the upwelling groundwater compared with that displayed in Figure 17c and d. The latter effect is due to a lower magnitude of hydrostatic damping factor applied to the hyporheic hydraulic head. Hence, the size of the discharge area at the streambed interface and the contribution of upward groundwater in stream water were larger in Figure 17c and d than they were in Figure 17a and b. However, in both cases, the discharge areas of regional groundwater flow decrease several orders of magnitude, which is discussed below (Figure 20).

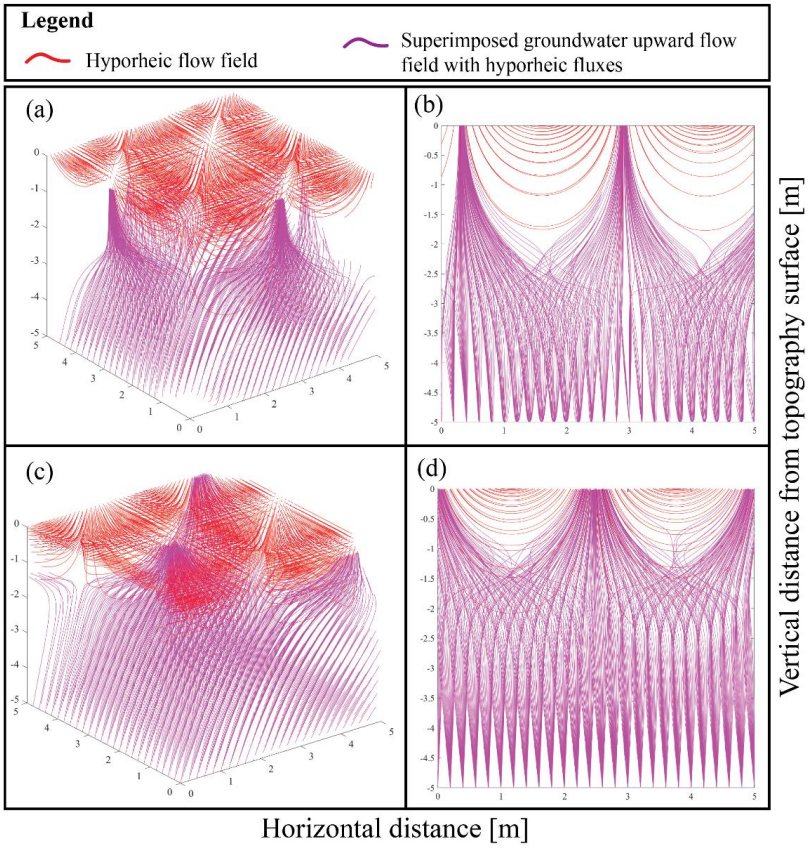

Figure 17. The impact of the hyporheic fluxes (red) on the upward groundwater flow (magenta) in the superimposed models (including both intermediate and deep groundwater flows). The figure corresponds to two arbitrary, superimposed cases of dynamic head coefficient of 0.08, (a) and (b): hydrostatic damping factor of 0.73; (c) and (d): hydrostatic damping factor of 0.13; (a) and (c): three-dimensional view; and (b) and (d): side view.

4.4.4 Size of subsurface flow discharge zone: Hyporheic and catchment groundwater

Fragmentation of coherent regional groundwater upwelling (i.e., $W_C>0$) and downwelling ($W_C<0$) zones at the streambed interface of the superimposed flow fields was defined by means of changes in a cumulative distribution function, CDF, due to the impact of hyporheic flow. A shift

of the CDF of the median values of regions (i.e., 50% of coherent upwelling/downwelling areas) toward smaller areas is referred to as a more fragmented upwelling or downwelling flow at the streambed interface. In Paper I, the fragmentation of both upwelling and downwelling regions of the superimposed flow field at the streambed interface were quantified for 5×5 m^2 regions for the corresponding flow behaviors of the first, second, third, and fifth stream orders. The distribution of up- and downwelling areas was normalized with the total area of the region, A_0, (25=5×5 m^2). The results indicated that the coherent downwelling areas are more fragmented than coherent upwelling regions in a superimposed flow field. The study demonstrated that considering a 4-m hyporheic depth and the damping factor estimated by Morén et al. (2017) for a fifth stream order created downwelling areas of less than 31% of the total area of the streambed (i.e., 7.75 m^2). Additionally, only 28% of the coherent upwelling zones have areas larger than 7.75 m^2 (Figure 18). The lower fragmentation of the upwelling areas compared with that of the downwelling areas is due to the choice of fifth stream order in this study. The results of a comparison between the fragmentation of upwelling and downwelling areas are presented in Figure 18 for the fifth-order stream, located downstream in the catchment with deep soil layers. The relatively higher hydraulic conductivity of existing soil type in the selected fifth-order segment compared with the first and second stream orders (located in headwaters) led to the domination of the gaining condition (Chen et al., 2013). The availability of a gaining or losing condition in a stream segment controls the physical and chemical properties of the aquatic sediment. Specifically, this factor impacts the fate of microbial transport between an aquifer and stream water (Franken et al., 2001).

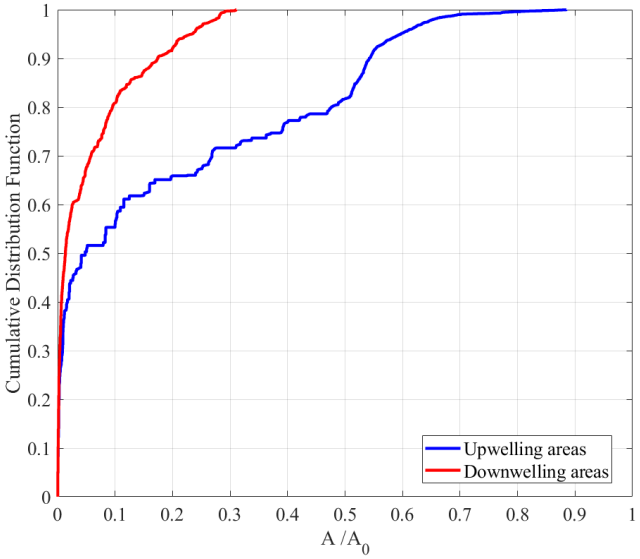

Figure 18. Cumulative distribution function of the size distribution of spatially coherent up- and downwelling areas for the fifth-order stream, assuming $R_{P,3}$ and ε = 4 m.

The impact of the groundwater flow field on the fragmentation of coherent upwelling hyporheic exchange fluxes at the streambed interface is of a great importance from a biological perspective. This is crucial when the degree of the upwelling zone fragmentation controls the temporal and spatial hotspots concerning biological activities within the aquatic sediment ecosystem (McClain et al., 2003). Paper I evaluated the impact of regional groundwater flow (representing first, second, third, and fifth stream orders) on the distribution of the coherent upwelling of hyporheic flow. The results demonstrated that the most fragmented upwelling areas belong to the hyporheic flow fields in the absence of groundwater flow. Superpositioning the catchment scale

groundwater with hyporheic flow decreased the fragmentation of upwelling areas, implying a shift of the area CDF toward larger areas. The change in the fragmentation of hyporheic upwelling areas due to the impact of groundwater flow impacts the stream water temperature and chemical properties of the stream sediments, which is induced by groundwater discharge. Additionally, the results highlighted the variation in the degree of fragmentation of upwelling areas among different stream orders. In particular, the fifth-order stream displayed the least fragmented areas, and the second-order stream had the most fragmented areas (Figure 19). Furthermore, the results highlighted the impacts of the hydrostatic damping factor and the depth of the hyporheic zone on the fragmentation of upwelling areas. The influence of hyporheic depth was found to be generally stronger than the hydrostatic damping factor. A deeper hyporheic zone decreased the magnitude of the hyporheic exchange flux, leading to a larger contribution of the catchment scale groundwater flow at the streambed interface. Similarly, the higher hydrostatic damping factor of the hyporheic hydraulic head decreased the hyporheic flow velocity and relatively increased the catchment scale groundwater contribution to discharge flow into surface water.

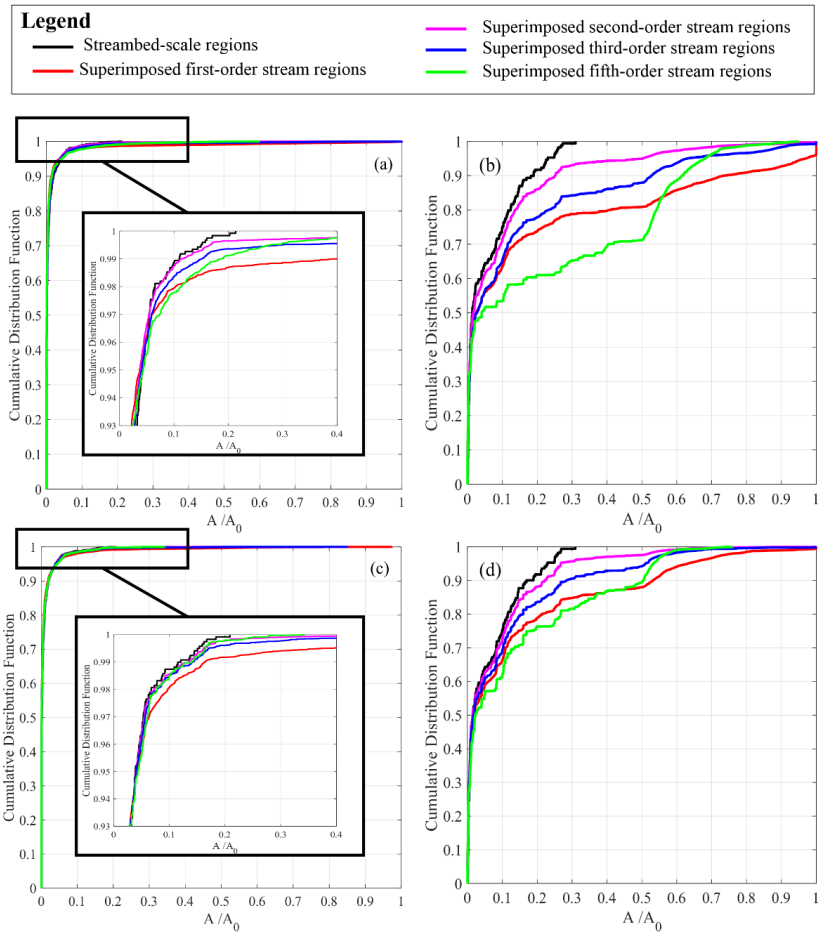

Figure 19. Cumulative distribution functions of the size distributions of spatially coherent upwelling areas for different stream orders assuming (a) $R_{p,2}$ and ε=0.1 m; (b) $R_{p,2}$ and ε=4 m; (c) $R_{p,4}$ and ε=0.1 m; and (d) $R_{p,4}$ and ε=4 m

The impact of hyporheic fluxes on the catchment scale groundwater discharge zones was investigated in Papers III and IV. The median coherent upwelling areas (without the impact of hyporheic fluxes near the bed surface) of the groundwater originating from a depth of 500 m and discharge at the stream bed surface were shown to be approximately 300 m^2 (or ~17 × 17 m^2), which is much larger than the size of the applied hyporheic model in this study (Paper IV). Additionally, superimposing the hyporheic flow field on the upwelling groundwater discharge zones substantially consolidated the upwelling groundwater flow into very small areas, forming pinholes of discharge at the streambed interface. The size of the upwelling groundwater flow discharge at the sediment–water interface is important in understanding the hydrological, biological, and ecological processes occurring within the aquatic sediment environment (Mathers et al., 2014; Fox et al., 2018). Additionally, one implication of the hyporheic flow on the groundwater discharge is the change of the residence time of radionuclide leakage from deep repository (carried by deep groundwater until the streambed sediment) within the aquatic sediment. The research conducted in Paper IV, showed that approximately 96% of the catchment scale groundwater flow had coherent upwelling areas larger than the total assumed hyporheic models (5×5 m^2) in the absence of hyporheic flow fields. On the other hand, the coherent upwelling areas of the hyporheic flow were always less than 7.5 m^2 (Figure 20). This reflects the stronger fragmentation behavior of hyporheic flow compared with that of regional groundwater flow at the streambed interface, which is associated with the different ranges of topographical scales controlling the two flows. Superimposing the hyporheic flow field on the subsurface groundwater flow significantly increased the fragmentation (i.e., shift of CDF toward the small areas) of the groundwater flow at the streambed interface. At this point, almost 95% of the superimposed flow field had coherent upwelling areas less than 1 m^2 at the top surface of the hyporheic model. This result was expected following the change in upward groundwater direction because of the existence of hyporheic fluxes which led to pinhole emergence within very small areas at the streambed interface. Thus, the groundwater flow was extremely fragmented due to the influence of existing hyporheic flow fields within the streambed sediment.

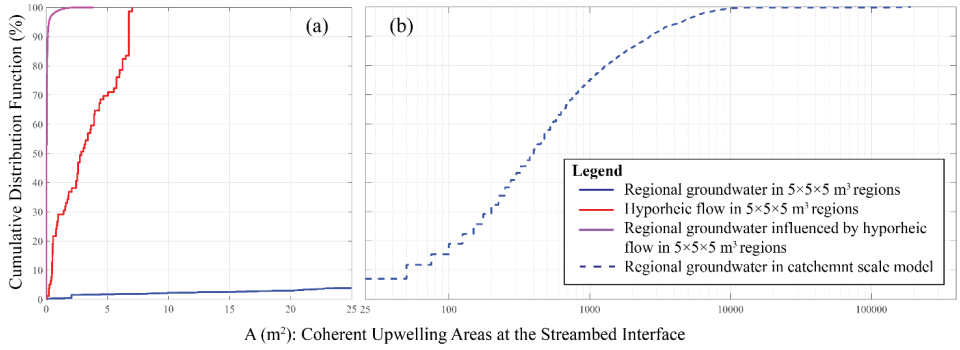

Figure 20. Cumulative distribution function plot of the coherent upwelling areas at the streambed interface for (a) groundwater flow (i.e., solid blue line), hyporheic exchange flow (i.e., solid red line), and groundwater flow influenced by hyporheic exchange fluxes (i.e., solid magenta line) in 5×5×5 m^3 regions; and (b) groundwater flow (dashed blue line) in catchment scale model

4.5 Characterizing the Characteristic Parameters of the Catchment

Principal component analysis (PCA) and power-law regression models were applied to find the best set of parameters describing the regional groundwater and hyporheic flow velocities at the streambed interface, as well as the ratio between them (Section 3.5). Additionally, internal covariance among various catchment properties was studied using the PCA (Paper I, V). Due to the variations among the range and magnitude of each individual parameter (several orders of

magnitude), the PCA was conducted on standardized parameters. The results of the PCA within standardized independent parameters demonstrated a complex internal covariance pattern in which six independent parameters were required to describe the internal covariance among different catchment properties (Paper I). A more detailed dataset (compared with Paper I) consisting of 24 variables was used in Paper V to represent independent geographic and hydrological catchment characteristics (Section 3.5). Next, a PCA was conducted to avoid multicollinearity between characteristic parameters and to reduce the number of independent parameters. This PCA in Paper V led to selection of 10 different characteristic parameters: standard deviation of landscape elevation, e_{std} (m); elevation gradient to the stream, GtS (-); subcatchment size, MCS (m^2); Darcy–Weibach friction factor, DW_{ff} (-); hydraulic conductivity of the soils, K (m/s); depth of Quaternary deposits, Z_Q (m); surface flow Reynolds number, Re (-); landscape topographical slope, S (-); level, SW_a (m), and slope, SW_b (-), of power spectral density of water surface profile (Figure 21). The results of the PCA confirmed the previous findings regarding the importance of topographic and geological parameters for the surface water–groundwater interaction (Tetzlaff et al., 2009; Sharma et al., 2015).

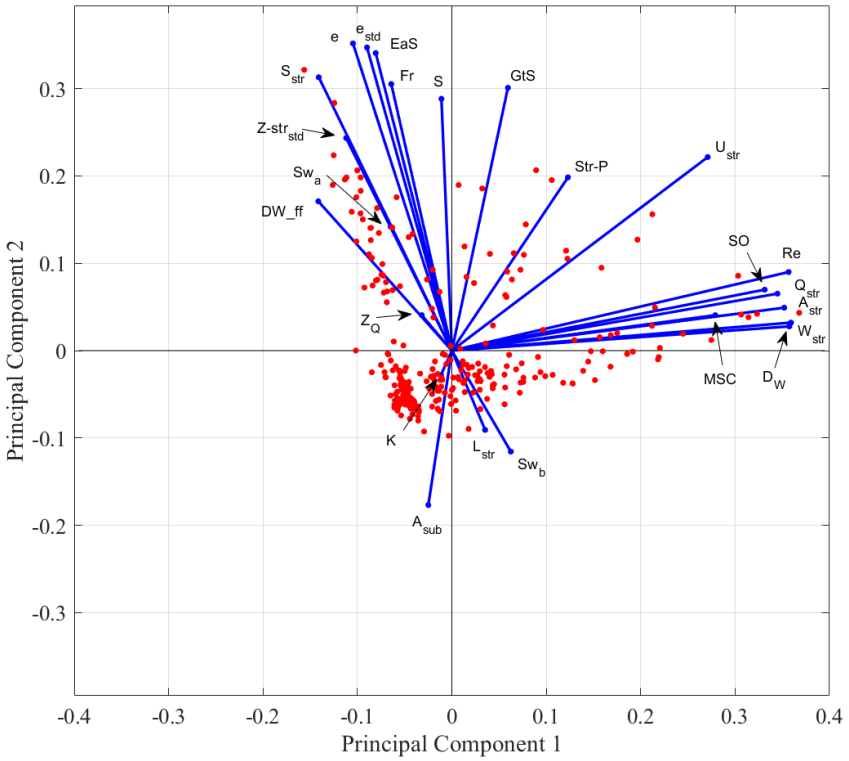

Figure 21. Principal component analysis results using the stream reach average for each standardized independent parameter (refer to Section 3.5 for the definitions of the notations)

In Paper V, all ten of the standardized independent parameters included in the PCA shown to impact groundwater-surface interaction were used in a multivariate power-law regression model (Equation 22). The results of the applied power-law statistical model demonstrated the major role of topographical parameters (GtS, MSC, S); geological factors (K and Z_Q); and the hydraulic parameters (SW_a, SW_b, Re) on the regional groundwater and the local hyporheic flow velocities as

well as the interaction between those two flow velocities at the streambed interface (Table 3). Notably, the 0.95 confidence level (P-value < 0.05) was used for all of the results in Table 3. The hydraulic conductivity played a significant role in deep groundwater discharge velocity in all the considered averaging scales (reach, intermediate subcatchment, and regional catchment scales). In addition to hydraulic conductivity, the reach slope, water surface elevation, and gradient of the stream displayed controlling effects on regional groundwater flow velocity. Furthermore, the local scale hydraulic parameters (SW_a and SW_b) substantially influenced the hyporheic exchange flow, as expected. The ratio between the regional groundwater water and hyporheic flows was revealed to be a function of the hydraulic parameters (SW_a and SW_b), hydraulic conductivity of the subsurface soil (K), and landscape topographical slope (S) depending on scale, on which the independent parameters were averaged. However, the performance of the evaluated functions for reach and intermediate subcatchment scales remained insignificant (0.41 and 0.49). Increasing the averaging scale (i.e., from reach scale toward the regional catchment scale) increased the performance of the model (i.e., R^2_{adj}) for all of the dependent variables. However, the results of the regional scale model might be uncertain due to the number of individual catchments considered in this study (only five individual catchments were used in evaluating the regional catchment scale functions).

Table 3. Best regression models at each averaging scale, based on the 0.95 confidence level and readjusted R^2-values of the independent variables and coefficients.

Dependent variable	Scale	Best regression model	$R^2_{adj.}$
Regional groundwater velocity	Reach	$W_C = (3.89 \times 10^{-4})\, K^{0.84} S^{1.22}$	0.30
	Intermediate subcatchment	$W_C = (79.4)\, K^{1} SW_a^{0.59}$	0.48
	Regional catchment	$W_C = (2.04 \times 10^{3})\, K^{1.32} GtS^{1.75}$	0.88
Hyporheic exchange velocity	Reach	$W_S = (6.85 \times 10^{-3})\, SW_a^{0.31} SW_b^{-1.864} K^{0.144}$	0.68
	Intermediate subcatchment	$W_S = (0.219)\, SW_a^{0.9}$	0.87
	Regional catchment	$W_S = (3.39 \times 10^{-4})\, GtS^{1.47} Z_Q^{0.61}$	0.98
Velocity ratio	Reach	$\frac{W_C}{W_S} = (1.66 \times 10^{-2})\, SW_a^{-0.28} SW_b^{3.55} K^{0.72} S^{1.07}$	0.45
	Intermediate subcatchment	$\frac{W_C}{W_S} = (0.865)\, SW_a^{1.48} SW_b^{13.05}$	0.32
	Regional catchment	$\frac{W_C}{W_S} = (8.71 \times 10^{5})\, S^{2.92} K^{1.57}$	0.97

4.6 The Impact of Flow Discharge on Hyporheic Depth

The spatial and temporal variations in stream water discharge controls the hyporheic flow exchange and substantially influences aerobic and anaerobic respiration in aquatic sediment (Trauth & Fleckenstein, 2017). In addition to the stream flow intensity, the heterogeneity in hydraulic conductivity of streambed sediment impacts the hyporheic exchange flow velocity and its penetration depth (Boano et al., 2008). Therefore, the impacts of flow discharge intensities on hyporheic exchange fluxes were analyzed using field experimental data and a numerical modeling approach (Paper II). The diurnal cycles of the surface water temperature were used to evaluate

the hyporheic flow depth. Additionally, difference between surface water and groundwater temperature provided the means to evaluate the contributions of upwelling groundwater in surface water during the field investigation (Anderson, 2005; Rau et al., 2010). Furthermore, the numerical modeling was used to analyze the variations in hyporheic depth, hyporheic water travel times, and fragmentation lengths (size distribution of coherent lengths with only upward or downward flow) of hyporheic flow at the streambed sediment interface induced by various discharge flow intensities during the experimental period for homogeneous and heterogeneous soil type materials.

4.6.1 Field investigation results

During the field investigation at the Krycklan catchment (Section 3.6), water temperature within the streambed sediment was recorded at seven different locations along the main river network of the experimental area during different flow discharges. The same experiment yielded nearly identical stream water temperatures (base-, low-, and high-flow conditions; Paper II). After this, the temperature data for all of the monitoring stations (seven location points) was used to present the temperature envelope along the depth of the streambed sediment (Figure 22). The temperature envelope represents the median (red line), and the 25th and 75th quartile range (shaded blue range) of the temperature recorded by each temperature sensor (i.e., each depth along individual MLTS) during different flow discharge intensities (refer to Table 2 in section 3.6.1 for the time period of each flow intensity). For example, the temperature envelope of low flow discharge at 150 m from the upstream lake (Figure 22b) represents the median (red line) and quartiles (shaded blue range) of the temperature from the MLTS at 150 m from the lake Stortjärn from August 7–19, 2017. These results are linearly interpolated along the depth (i.e., sensor). Since the field measurement was conducted during the summer, the water temperature within the hyporheic zone decreased with depth (Shanafield et al., 2011). Generally, the surface water has higher temperature than the subsurface flow throughout the summer. Therefore, the amplitudes of the diurnal temperature signal were progressively damped with depth due to the interaction between cold upward groundwater near the streambed surface and warm downward surface water flow within the sediment through the thermal dispersion which is associated with hydrodynamic dispersion and thermal diffusion (Conant, 2004). Additionally, the temperature envelope shows the temperature change with depth, where there is a gradual incline in median value and an abrupt shift of the quartile range (i.e., between the 25th and 75th values represented by the blue shaded range) to a narrow range of temperature. This result suggests the existence of intense hyporheic flow and more significant influence of groundwater discharge deeper within the sediment profile (at 550, 620, 975, and 1100 m from the upstream station). This temperature pattern implies a shallow (i.e., up to 10 cm) hyporheic zone that bounds with cold upward groundwater fluxes at the bottom. On the other hand, the strong temperature gradient with a wide range of temperature quartile in depth reflects a substantial convective heat transport via downward surface water through the sediment profile (150, 200, and 350 m from the upstream station). Additionally, a shallow hyporheic zone can be interpreted using the temperature variability in top aquatic sediment at 550 and 975 m from the upstream station. Generally, the groundwater has a relatively uniform temperature through the entire year, ranging between 8 and 12 °C; whereas the temperature of the surface water significantly varies throughout the year and even on a single day. Considering the time and location of the field experiment (summer time in Sweden), the surface water temperature was in the range of 13–17 °C. The recorded temperature during low flow is in the range of 8–12 °C along all the temperature profiles, revealing the existence of upward groundwater flow for all the monitoring stations in the absence for surface water (Figure 22). Furthermore, the very wide variation in temperature profile along the depth during the high flow discharge resulted from the sharp incremental change in water temperature, which was experienced upon the arrival of the flood wave. Finally, the results of the temperature

field measurement in this study confirm Leach et al.'s (2017) findings regarding upwelling and downwelling reaches along the stream segment.

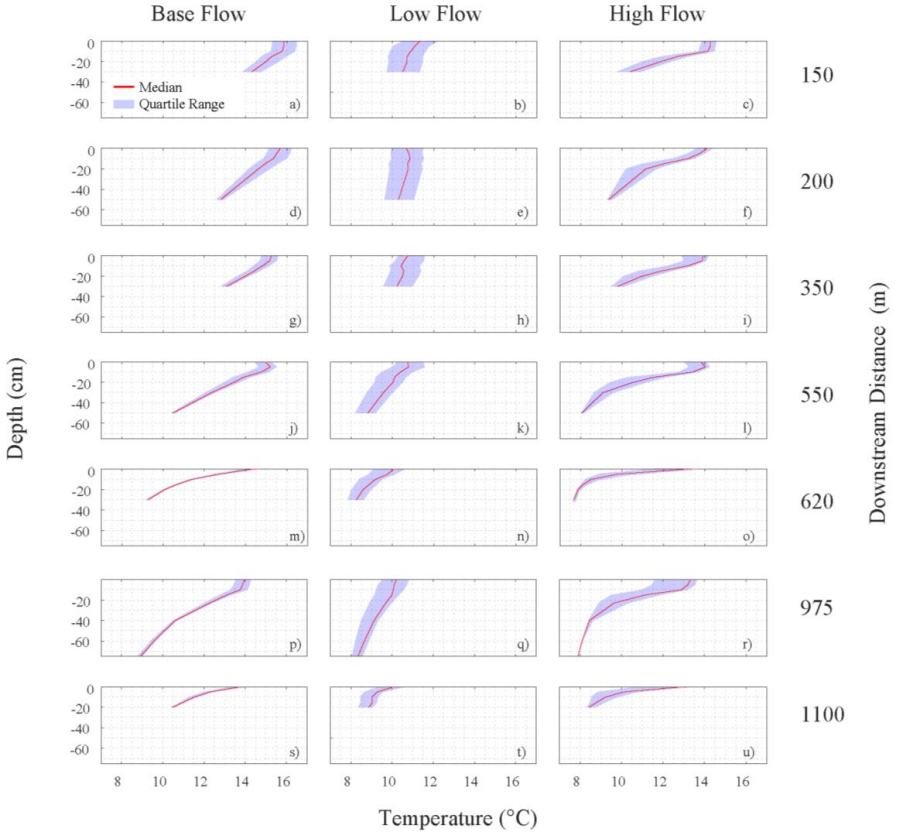

Figure 22. Vertical envelopes of temperature dynamics during base-, low-, and high-flow stream discharges (discharge values presented in Table 2, Section 3.6.1) at different monitoring locations. The envelopes indicate the interquartile range (shaded area) and the median (red line).

4.6.2 Numerical results

The numerical modeling of the field investigation data (Section 3.6.2) aims to identify the hyporheic exchange flow pattern under different flow conditions and to evaluate the interaction between surface water and groundwater with different hypothetical geological properties. The impact of various flow discharge intensities on hyporheic depth was investigated by assessing the maximum penetration depth of the surface water flow into the sediment, $D_{HF,\ max}$ and the residence time of hyporheic fluxes, τ. Due to the strong impact of geological properties of the subsurface soil on the hyporheic exchange fluxes (Cardenas et al., 2004; Salehin et al., 2004), the distributions of $D_{HF,\ max}$ and τ were presented for two different sediment materials. These were as follows: (a) the constant hydraulic conductivity for both sediment (i.e., top 1 m of the subsurface) and the underlying soil and (b) the depth-decaying hydraulic conductivity of the sediment and constant hydraulic conductivity of the underlying soil. Figure 23 shows that the interquartile of $D_{HF,\ max}$ has approximately the same range for all of the flow conditions for each of the considered soil hydraulic conductivity values. However, the median value of $D_{HF,\ max}$ slightly differs with discharge intensities, and the low-flow discharge had the deepest maximum depth of hyporheic flow field. This result was because the higher variation in water surface elevation acted

as a hydraulic head top boundary condition during low-flow discharge, which did not happen at other flow discharge intensities. The results highlighted the role of hydraulic conductivity in the subsurface soil where the depth-decaying hydraulic conductivity significantly decreased the hyporheic depth (approximately two orders of magnitude). The hyporheic zone's depth decreased because of the larger shielding impact due to lower hydraulic conductivity as the depth increased (Gomez-Velez et al., 2014). The hyporheic zone had the depth in the order of centimeter scale based on depth-decaying hydraulic conductivity, whereas assuming constant hydraulic conductivity of the subsurface material led to hyporheic depth in the order of meter scale.

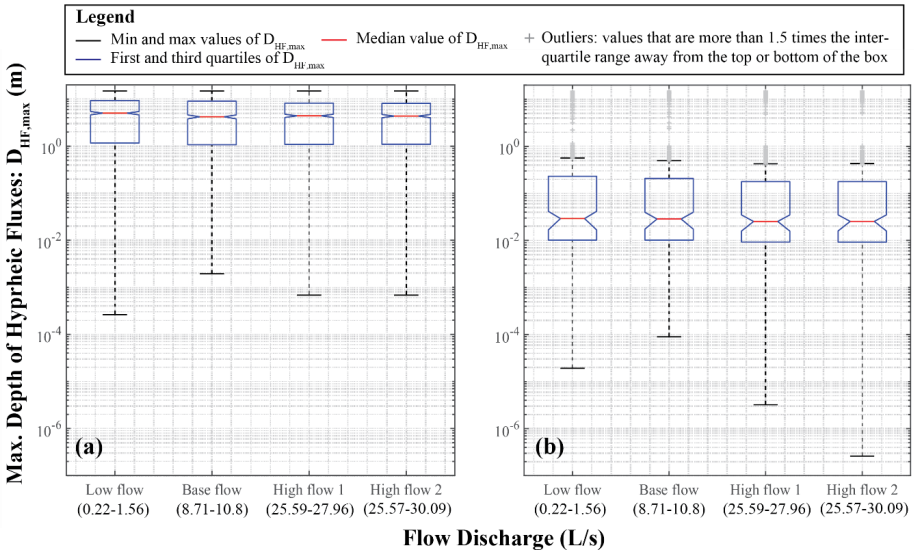

Figure 23. Boxplots showing the maximum depth of hyporheic fluxes under various flow discharges assuming (a) constant hydraulic conductivity ($K = 10^{-4}$ [m/s]) for the entire subsurface region and (b) a decaying hydraulic conductivity (starting from $K(Z = 0) = 10^{-4}$ [m/s] at the surface–subsurface water interface and decaying exponentially to $K(Z = -1) = 10^{-7}$ [m/s] at one meter deep. In the case of a vertically varying hydraulic conductivity, a constant hydraulic conductivity ($K = 10^{-7}$ [m/s]) was used for depths greater than one meter. The second row of the horizontal axis (i.e., numbers) includes the ranges of stream-flow discharge along the stream for each flow regime. Finally, $D_{HF,max}$ is the deepest point of the streamlines.

The hyporheic flow residence time depends on channel morphology, the saturated hydraulic conductivity of subsurface soil, the head gradient over the bedform, and the flow trajectory in the subsurface domain. Additionally, the distribution of hyporheic flow residence time was estimated using the applied particle tracing method (Section 3.6.2). Here the residence time was defined as the time spent by each particle moving from the streambed interface into the subsurface domain until returning to the streambed surface again. The relatively small spatial variation of water surface elevation between different discharge intensities along the stream channel led to approximately similar wavelengths of the top head boundary condition (Kasahara & Wondzell, 2003). Consequently, the subsurface flow trajectories and the residence time of the hyporheic flows varied slightly across different stream water discharge intensities. The distribution of water residence times in the hyporheic zone controls the rate of the nitrification and denitrification processes in streams with nitrogen transport. Thus, the high and low rates of nitrifications occur at short and long residence times, respectively (Zarnetske et al., 2011). The ways the stream

discharge affected the distribution of residence time, τ, demonstrated that the high discharge had the greatest range of hyporheic flow residence times regardless of considered hydraulic conductivity value (Figure 24). The wide range of hyporheic flow residence times imply the existence of a more complex hyporheic flow trajectory network consisting of hyporheic flows with different spatial scales induced by high-flow discharge, important for biogeochemical cycling (Ward et al., 2013). On the other hand, the low-flow discharge had the shortest range of hyporheic residence times, reflecting the existence of hyporheic flow with a relatively uniform flow trajectory pattern. Beyond this, high-flow discharge intensities always induced the minimum residence time. Comparing the hyporheic flow residence times between the two applied hydraulic conductivities of the subsurface material indicated higher τ values upon applying the depth-decaying hydraulic conductivity. The median values of hyporheic flow residence time are quite long in all of the flow discharges, regardless of the applied hydraulic conductivity scenario. This phenomenon is due to the relatively small variations in the measured water levels for each of the individual discharge intensities along the stream network and the relatively long (50 m spatial interval) distance between the surface water level observational stations. This effect led to long hyporheic flow trajectories within the subsurface region.

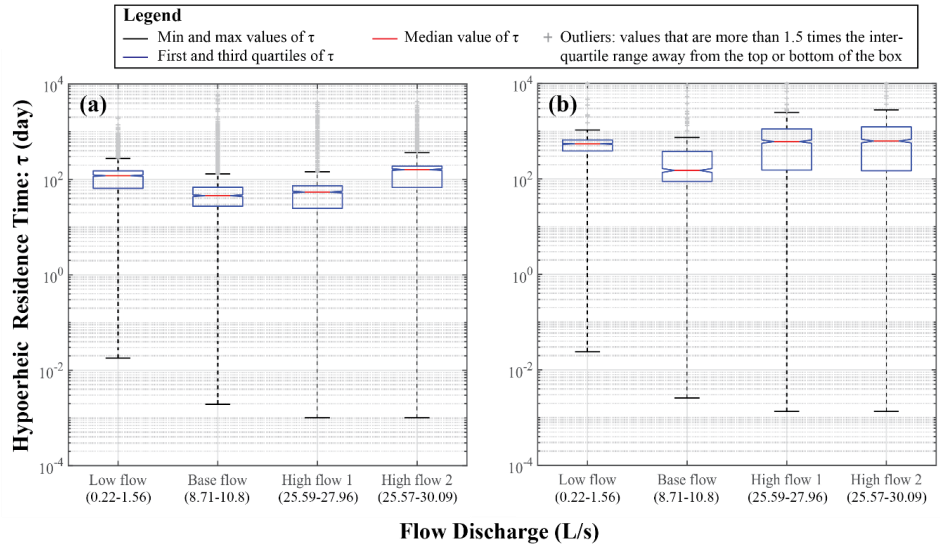

Figure 24. Box and whisker plots of hyporheic fluxes' residence times under various flow discharges assuming (a) constant hydraulic conductivity ($K = 10^{-4}$ [m/s]) for the entire subsurface region and (b) decaying hydraulic conductivity (starting from $K(Z = 0) = 10^{-4}$ [m/s] at the surface–subsurface water interface and decaying exponentially to $K(Z = -1) = 10^{-7}$ [m/s] down to a depth of 1 m). In the case of vertically varying hydraulic conductivity, a constant hydraulic conductivity ($K = 10^{-7}$[m/s]) was used for depths greater than 1 m. The second row of the horizontal axis (numbers) shows the ranges of stream flow discharge along the stream for each flow regime. Finally, τ is the residence time of the particles released at the streambed interface.

4.7 Applications

The groundwater travel times of the hierarchical nested subsurface flow system influence the physical and chemical properties of the subsurface water across the range of spatio-temporal scales. Thus, these times impact ecosystems of the subsurface and surface water, especially at groundwater discharge locations. For instance, previous studies have been argued the controlling

impact of fertilizer infiltration from agriculture land on eutrophication rate in recipient water (Hoffmann et al., 2006; Gelbrecht et al., 2005). Groundwater is the main transport agent for natural solutes and contaminants in the subsurface domain and controls the exchange of solutes and contamination between the aquifer and the surface water resources. Therefore, investigating the groundwater–surface water interactions from different technical angles provided essential knowledge on the transportation and accumulation of the solutes and contaminants close to the topography surface that may impact the ecosystem, endangering the environment and living biota. In particular, the radioactive compound dose assessment substantially depends on one's understanding of the subsurface flow process from a great depth to far shallower, localized flow interactions. The new understanding of groundwater-surface water interaction presented in this study addresses the technical issues related to radionuclide contamination transport that leaked from HLRW repository and discharges into the surface water bodies.

This thesis presents a quantitative analysis on regional groundwater flow circulation considering site-specific hydrological and geological data in Sweden. Analyses of radioactive contamination transport require a compartment modeling approach (Avila et al., 2010), where the groundwater flow results reflecting the flow within and between the biospheres and geospheres provide a basis for these analyses. The results of this study could be used to advance understanding of radioactive contamination's fate and transport close to the surface which is of a great importance in safety assessment programs. The importance of groundwater–surface water interaction has been extensively discussed (Fleckenstein et al., 2010; Wondzell, 2015), whereby especially the temporal and spatial fluctuations in surface water and groundwater levels require complex numerical and statistical analyses. The results of this study could help researchers relate the variability in stream water discharge values to groundwater–surface water interaction. Furthermore, this study addressed the main drivers of groundwater flow circulation, such as fractal topography, structural layers of subsurface geological formations, and the impact of depth-decaying hydraulic conductivity. Finally, the link between geographical and hydrogeological parameters to regional and hyporheic flows represents a major advancement in understanding of the deep and shallow subsurface flow renewal rate, which has implications for long term freshwater resources management.

4.8 Limitations and Future Prospects

This thesis presents multiscale subsurface flow modeling by separately developing regional and hyporheic scale models and then superimposing the flow fields from different spatial scale intervals. The applied multiscale approach evaluated regional groundwater and hyporheic flows at the sediment–bed interface through numerical modeling of the catchment scale groundwater and exact solution to hyporheic hydraulic heads. Before this study, evaluating the interaction between groundwater flow and hyporheic exchange flow had not been conducted using the detailed applied method here. For this reason, this method is an advancement in the hierarchically nested subsurface flow system modeling focused on the discharge zones of regional groundwater. In particular, the influence of hyporheic fluxes on deep groundwater flow within the aquatic sediment had been neglected in previous literature. Therefore, the following suggestions are provided for advancing subsurface flow simulation further and improving understanding of surface water–groundwater interactions:

- **Conducting a sensitivity analysis on the topographical DEM resolution to find a generally variable resolution that satisfies the infiltration constraint.** In this study, an innovative variable DEM resolution was introduced to satisfy both of the topography-controlled head in the discharge areas with surface water objects and otherwise recharge controlled head with lower DEM resolution consistent with the appropriate infiltration rate. However, the analysis was performed for only one catchment. Thus, it is recommended that the method be applied to different catchments with different hydrogeological properties to prepare a guideline for DEM preparation prior to

groundwater modeling. Such work would be especially useful in establishing the connection between variable DEM resolution and infiltration rate under different hydrogeologic conditions.

- **Improve groundwater-surface water interaction in lake sediments**. In this study the surface water objects were characterized using the applied bi-modality approach (i.e., changing the DEM resolution to simulate the recharge-controlled boundary condition over the surface water bodies). Consequently, lakes and streams were treated similarly in the analyses and the role of thermo-stratified water and stagnant water level of lakes in groundwater-surface water interaction were not investigated.
- **Improve the regional groundwater model using more observational data.** The applied method in groundwater modeling could be strengthened by using more detailed observational data, including the spatial and temporal variations in porosity and hydraulic conductivity values of aquatic sediment, QD and bedrock domains, and the existence of fracture networks in bedrock. Additionally, observational groundwater hydraulic heads could be used to validate the modeled groundwater surface.
- **Improve the topographical data applied in hyporheic scale modeling.** Due to the lack of general streambed topographic data, this study applied a rescaling method to represent the hyporheic scale topography. As an alternative method, high-resolution measured topography values over larger parts of the stream network would be suitable for hyporheic scale modeling and to improve the evaluation of hyporheic flows without using rescaling methods.
- **Conducting field investigations for improved estimation of the hydrostatic damping factor and dynamic coefficient of the hydraulic head at the streambed interface.** More field investigations are needed in different regions with different stream flow types and physical characteristics of channel morphology. Additionally, various geological properties should be used to find a general pattern for the range of possible hydrostatic damping factors and dynamic coefficients.
- **Investigation of temporal variations in groundwater–surface water interaction.** Climate fluctuation appears on seasonal, biannual, and decadal timescales, leading to temporal fluctuations in aquifers and groundwater flow circulation. Thus, considering the temporal variation in infiltration provides an enhanced picture of groundwater–surface water interactions.

5 SUMMARY AND CONCLUSION

This thesis investigated the role of hyporheic exchange fluxes in hierarchically nested groundwater flow systems, especially in regional groundwater discharge zones in surface water. A multiscale numerical modeling approach and field investigations were conducted on a boreal Swedish catchment to account for the groundwater flow and the hydrogeological and morphological properties of the catchment. The main objectives were to apply the multiscale modeling platform to assess the impacts of hyporheic exchange fluxes on deep groundwater discharge within the nested flow system within the aquatic sediment and the reverse effect of the regional groundwater flow on the hyporheic flow. Thus, the study produced the following conclusions:

1. The catchment's landscape topography controls the groundwater flow circulation in areas where the ratio of infiltration rate to subsurface soil hydraulic conductivity is relatively high. This condition leads to saturated subsurface regions, where the hydraulic head distribution over the catchment is a subdued replica of the topographic elevation and follows the landscape gradient. Such regions are known as areas with topography-controlled groundwater flow. On the other hand, the groundwater hydraulic head does not

follow the topographic surface in areas with low ratios of infiltration rate to soil hydraulic conductivity, leading to the development of unsaturated subsurface soil. These areas are called recharge-controlled regions, where the groundwater hydraulic head variation is typically smoother than the fluctuation in topography elevation. One way to deal with this situation in groundwater flow modeling would be to lower the resolution of the groundwater table topography by smoothing the fluctuation in landscape topography elevation. In this thesis, DEM files with lower mesh size resolution than the real measured topography were applied at downwelling areas to compare them to upwelling areas to investigate the validity and implication of this hypothesis. The results of this thesis highlighted the role of topography elevation resolution in satisfying the topography- and recharge-controlled boundary conditions in a single model. In this study, the results showed that the appropriate DEM resolutions for the study domain are 84 m at downwelling regions (terrain with high local elevation), which provided approximately the same infiltration as the observations. Notably, the appropriate resolution of DEM file substantially depends on climatic and geologic conditions of the catchment and differs across different regions.

2. The existence of fractal patterns in landscape topography allows one to generalize observed topography beyond observed scale intervals. Furthermore, exact spectral solutions to the groundwater flow problem can be applied based on the evaluation of the amplitudes and wavelengths of real Fourier series representing topography elevations. At this point, the prevailing of the fractal power across different spatial scales of the landscape topography were generalized into higher resolution (smaller size) of the streambed topography and applied to the hyporheic flow modeling. The hyporheic hydraulic head at the streambed consists of hydrostatic and dynamic head contributions, both of which can be described using the streambed topography variations. The results indicated the hydrostatic head component is generally much higher than the dynamic head component. Additionally, the results showed that Froude number controls both the hydrostatic and dynamic head contributions, meaning that their relative importance can vary significantly across time and space.
3. Numerical modeling was used to investigate the regional groundwater, accounting for subsurface heterogeneity, such as different subsurface strata (i.e., sediments, Quaternary deposits, and bedrock). In particular, depth-decaying hydraulic conductivity was considered for different layers of the subsurface where the specific hydraulic conductivities of the different soil types were considered for the Quaternary deposits. The results of this thesis indicated that the depth-decaying hydraulic conductivity reduces the groundwater flow circulation increasingly with depth. One application of the research in this study is understanding how deep groundwater flow carries radioactive compounds leaking from an HLRW and discharges them into surface water. This process affects both groundwater circulation and the chemical retardation due to adsorption in different geological strata. The adsorption retardation coefficient significantly varies across different subsurface domains and controls the fate and transport of radionuclide compound. In particular, this process leads to the same range of contamination's residence times in soil and bedrock (i.e., median residence time in the range of 5,000–8,000 years). Additionally, the results demonstrated that the deep groundwater discharge zones are aligned well with natural drainage (i.e., stream networks and lakes) and the topography elevation of the catchment. More specifically, the majority of the discharge zones were located on the topography surface in the downstream part of the catchment area containing relatively deeper Quaternary deposit and soil types with higher permeability values.
4. The upward groundwater flow reduces the hyporheic exchange flow depth and affects its discharge pattern. The magnitude of hyporheic fluxes were found to be at least one order

of magnitude higher than the groundwater flow at the streambed interface that led to the domination of hyporheic fluxes immediately below the streambed. Beyond this, the fragmentation of coherent upwelling zones at the streambed interface was significantly impacted by discharging groundwater. The coherent upwelling areas of the hyporheic flow were always found to be less than 31% of the hyporheic scale model's top surface (in the absence of groundwater flow). At the same time, the groundwater flow substantially decreased the degree of fragmentation (shift of the CDF plot toward higher areas) of the coherent upwelling area for the hyporheic flow.

5. The results of this study revealed significant effects on groundwater travel times in aquatic sediments induced by hyporheic flow fields. The travel times of both the intermediate and deep groundwater flows were reduced by 50% compared with those of a case that lacked hyporheic flow. Additionally, the upwelling groundwater flow areas within the streambed sediment substantially contracted into small areas (less than 5 m^2) due to the impact of the hyporheic flow field. This phenomenon was depicted as a pinhole discharge phenomenon resulting at the streambed interface due to the impact of hyporheic flow. The hydraulic conductivity decay, the ratio of regional groundwater to hyporheic flow velocities, and the heterogeneity of the streambed sediment controlled the convergence behavior of the groundwater flow. Furthermore, the contraction of groundwater flow into small, fragmented areas at the sediment bed interface and the longer travel times of the upward groundwater flow within the aquatic sediment due to the impact of hyporheic fluxes are important for heat, solute, and contaminant transport from aquifer to stream water, substantially affecting the streambed sediment and surface water ecology. Another implication of this effect is that the radionuclide transfer rate coefficient applied to ecological compartment models increases due to the impact of the hyporheic flow field, which could affect the risk of radiological doses for humans.
6. A field campaign was performed to investigate the impact of flow discharge intensities representing low-, base-, and high-flow conditions on hyporheic exchange flow. Heat was used as a natural trace element to evaluate gaining (upward flow direction) and losing (downward flow direction) segments along the stream network. The temperature profile measured along the hyporheic depth showed a deeper hyporheic zone when the discharge intensity increased. The numerical modeling results revealed that increasing the flow discharge intensity led to an increased interquartile range of hyporheic flow residence times. Additionally, the numerical modeling results highlighted the major role of subsurface hydraulic conductivity on the depth of a hyporheic zone and the hyporheic residence time within the subsurface domain.
7. The conducted PCA and (parametric) regression analysis results evaluated the role of various parameters in generalizing the groundwater–surface water interaction. The results demonstrated that the landscape topographical slope, hydraulic conductivity and depth of soil layer, and the level and slope of the power spectral density of the water surface profile have controlling effects on the magnitude of groundwater flow and hyporheic exchange flow velocities. These components also affect the interaction between groundwater and hyporheic exchange flow; which could be important for generalization of the flow results.

References

Anderson, M. P. (2005). Heat as a ground water tracer. *Groundwater*, *43*(6), 951-968.

Avila, R., Ekström, P. A., & Åstrand, P. G. (2010). *Landscape dose conversion factors used in the safety assessment SR-Site* (No. SKB-TR-10-06). Swedish Nuclear Fuel and Waste Management Co..

Avila, R., Kautsky, U., Ekström, P. A., Åstrand, P. G., & Saetre, P. (2013). Model of the long-term transport and accumulation of radionuclides in future landscapes. *Ambio*, *42*(4), 497-505. https://doi.org/10.1007/s13280-013-0402-x

Bear, J. (2012). *Hydraulics of groundwater*. Courier Corporation.

Bencala, K. E. (1983). Simulation of solute transport in a mountain pool-and-riffle stream with a kinetic mass transfer model for sorption. *Water Resources Research*, *19*(3), 732-738.

Bhaskar, A. S., Harvey, J. W., & Henry, E. J. (2012). Resolving hyporheic and groundwater components of streambed water flux using heat as a tracer. *Water Resources Research*, *48*(8).

Blazkova, S., Beven, K., Tacheci, P., & Kulasova, A. (2002). Testing the distributed water table predictions of TOPMODEL (allowing for uncertainty in model calibration): The death of TOPMODEL?. *Water Resources Research*, *38*(11), 39-1.

Boano, F., Revelli, R., & Ridolfi, L. (2008). Reduction of the hyporheic zone volume due to the stream-aquifer interaction. *Geophysical Research Letters*, *35*(9).

Boano, F., Revelli, R., & Ridolfi, L. (2009). Quantifying the impact of groundwater discharge on the surface–subsurface exchange. *Hydrological Processes: An International Journal*, *23*(15), 2108-2116. https://doi.org/10.1002/hyp.7278

Boano, F., Harvey, J. W., Marion, A., Packman, A. I., Revelli, R., Ridolfi, L., & Wörman, A. (2014). Hyporheic flow and transport processes: Mechanisms, models, and biogeochemical implications. *Reviews of Geophysics*, *52*(4), 603-679.

Boulton, A. J., & Hancock, P. J. (2006). Rivers as groundwater-dependent ecosystems: a review of degrees of dependency, riverine processes and management implications. *australian Journal of Botany*, *54*(2), 133-144.

Boulton, A. J., Datry, T., Kasahara, T., Mutz, M., & Stanford, J. A. (2010). Ecology and management of the hyporheic zone: stream–groundwater interactions of running waters and their floodplains. *Journal of the North American Benthological Society*, *29*(1), 26-40.

Cardenas, M. B., Wilson, J. L., & Zlotnik, V. A. (2004). Impact of heterogeneity, bed forms, and stream curvature on subchannel hyporheic exchange. *Water Resources Research*, *40*(8).

Cardenas, M. B., & Wilson, J. L. (2006). The influence of ambient groundwater discharge on exchange zones induced by current–bedform interactions. *Journal of Hydrology*, *331*(1-2), 103-109. https://doi.org/10.1016/j.jhydrol.2006.05.012

Cardenas, M. B., & Wilson, J. L. (2007). Exchange across a sediment–water interface with ambient groundwater discharge. *Journal of hydrology*, *346*(3-4), 69-80.

Cardenas, M. B. (2008). Surface water-groundwater interface geomorphology leads to scaling of residence times. *Geophysical Research Letters*, *35*(8).

Cardenas, M. B., & Jiang, X. W. (2010). Groundwater flow, transport, and residence times through topography-driven basins with exponentially decreasing permeability and porosity. *Water Resources Research*, *46*(11).

Cardenas, M. B. (2015). Hyporheic zone hydrologic science: A historical account of its emergence and a prospectus. *Water Resources Research*, *51*(5), 3601-3616.

Carucci, V., Petitta, M., & Aravena, R. (2012). Interaction between shallow and deep aquifers in the Tivoli Plain (Central Italy) enhanced by groundwater extraction: a multi-isotope approach and geochemical modeling. *Applied Geochemistry*, *27*(1), 266-280.

Caruso, A., Ridolfi, L., & Boano, F. (2016). Impact of watershed topography on hyporheic exchange. *Advances in water resources*, *94*, 400-411.

Chen, X., Dong, W., Ou, G., Wang, Z., & Liu, C. (2013). Gaining and losing stream reaches have opposite hydraulic conductivity distribution patterns. *Hydrology and Earth System Sciences*, *17*(7), 2569-2579.

Conant Jr, B. (2004). Delineating and quantifying ground water discharge zones using streambed temperatures. *Groundwater*, *42*(2), 243-257.

Conant Jr, B., Cherry, J. A., & Gillham, R. W. (2004). A PCE groundwater plume discharging to a river: influence of the streambed and near-river zone on contaminant distributions. *Journal of Contaminant Hydrology*, *73*(1-4), 249-279.

Desbarats, A. J., Logan, C. E., Hinton, M. J., & Sharpe, D. R. (2002). On the kriging of water table elevations using collateral information from a digital elevation model. *Journal of Hydrology*, *255*(1-4), 25-38.

Devito, K., Creed, I., Gan, T., Mendoza, C., Petrone, R., Silins, U., & Smerdon, B. (2005). A framework for broad-scale classification of hydrologic response units on the Boreal Plain: Is topography the last thing to consider?. *Hydrological Processes: An International Journal*, *19*(8), 1705-1714. https://doi.org/10.1002/hyp.5881

Duff, J. H., & Triska, F. J. (1990). Denitrifications in sediments from the hyporheic zone adjacent to a small forested stream. *Canadian Journal of Fisheries and Aquatic Sciences*, *47*(6), 1140-1147.

Elliott, A. H., & Brooks, N. H. (1997a). Transfer of nonsorbing solutes to a streambed with bed forms: Theory. *Water Resources Research*, *33*(1), 123-136.

Elliott, A. H., & Brooks, N. H. (1997b). Transfer of nonsorbing solutes to a streambed with bed forms: Laboratory experiments. *Water Resources Research*, *33*(1), 137-151.

Ericsson, L. O., Holmen, J., Rhen, I., & Blomquist, N. (2006). *Supra regional ground water modelling-in-depth analysis of the groundwater flow patterns in eastern Smaaland. Comparison with different conceptual descriptions* (No. SKB-R--06-64). Swedish Nuclear Fuel and Waste Management Co.. Retrieved from https://inis.iaea.org/collection/NCLCollectionStore/_Public/37/069/37069026.pdf?r=1

Fehlman, H. M. (1985), Resistance components and velocity distributions of open channel flows over bedforms, M.S. thesis, Colorado State University, Fort Collins, Colorado.

Fleckenstein, J. H., Krause, S., Hannah, D. M., & Boano, F. (2010). Groundwater-surface water interactions: New methods and models to improve understanding of processes and dynamics. *Advances in Water Resources*, *33*(11), 1291-1295.

Franken, R. J., Storey, R. G., & Williams, D. D. (2001). Biological, chemical and physical characteristics of downwelling and upwelling zones in the hyporheic zone of a north-temperate stream. *Hydrobiologia*, *444*(1), 183-195.

Fox, A., Boano, F., & Arnon, S. (2014). Impact of losing and gaining streamflow conditions on hyporheic exchange fluxes induced by dune-shaped bed forms. *Water Resources Research*, *50*(3), 1895-1907.

Fox, A., Laube, G., Schmidt, C., Fleckenstein, J. H., & Arnon, S. (2016). The effect of losing and gaining flow conditions on hyporheic exchange in heterogeneous streambeds. *Water Resources Research*, *52*(9), 7460-7477.

Fox, A., Packman, A. I., Boano, F., Phillips, C. B., & Arnon, S. (2018). Interactions between suspended kaolinite deposition and hyporheic exchange flux under losing and gaining flow conditions. *Geophysical Research Letters*, *45*(9), 4077-4085. https://doi.org/10.1029/2018GL077951

Gelbrecht, J., Lengsfeld, H., Pöthig, R., & Opitz, D. (2005). Temporal and spatial variation of phosphorus input, retention and loss in a small catchment of NE Germany. *Journal of hydrology*, *304*(1-4), 151-165.

Gomez-Velez, J. D., Krause, S., & Wilson, J. L. (2014). Effect of low-permeability layers on spatial patterns of hyporheic exchange and groundwater upwelling. *Water Resources Research*, *50*(6), 5196-5215.

Gomez-Velez, J. D., Harvey, J. W., Cardenas, M. B., & Kiel, B. (2015). Denitrification in the Mississippi River network controlled by flow through river bedforms. *Nature Geoscience*, *8*(12), 941-945.

Haitjema, H. M., & Mitchell-Bruker, S. (2005). Are water tables a subdued replica of the topography?. *Groundwater*, *43*(6), 781-786.

Harvey, J. W., & Bencala, K. E. (1993). The effect of streambed topography on surface-subsurface water exchange in mountain catchments. *Water resources research*, *29*(1), 89-98.

Harvey, J. W., Wagner, B. J., & Bencala, K. E. (1996). Evaluating the reliability of the stream tracer approach to characterize stream-subsurface water exchange. *Water resources research*, *32*(8), 2441-2451.

Hedin, A. (2006). *Long-term safety for KBS-3 repositories at Forsmark and Laxemar-a first evaluation. Main Report of the SR-Can project* (No. SKB-TR--06-09). Swedish Nuclear Fuel and Waste Management Co..

Hoffmann, C. C., Berg, P., Dahl, M., Larsen, S. E., Andersen, H. E., & Andersen, B. (2006). Groundwater flow and transport of nutrients through a riparian meadow–field data and modelling. *Journal of Hydrology*, *331*(1-2), 315-335.

Holmén, J. G., Stigsson, M., Marsic, N., & Gylling, B. (2003). *Modelling of groundwater flow and flow paths for a large regional domain in northeast Uppland. A three-dimensional, mathematical modelling of groundwater flows and flow paths on a super-regional scale, for different complexity levels of the flow domain* (No. SKB-R--03-24). Swedish Nuclear Fuel and Waste Management Co..

Ingebritsen, S. E., & Manning, C. E. (1999). Geological implications of a permeability-depth curve for the continental crust. *Geology*, *27*(12), 1107-1110. https://doi.org/10.1130/0091-7613(1999)027<1107:GIOAPD>2.3.CO;2

Jakubick, A. T. (1979). Analysis of Pu-Release Consequences on the Environmental Geochemistry. In *Scientific Basis for Nuclear Waste Management* (pp. 427-434). Springer, Boston, MA.

Jerolmack, D., & Mohrig, D. (2005). Interactions between bed forms: Topography, turbulence, and transport. *Journal of Geophysical Research: Earth Surface*, *110*(F2).

Jiang, X. W., Wan, L., Wang, X. S., Ge, S., & Liu, J. (2009). Effect of exponential decay in hydraulic conductivity with depth on regional groundwater flow. *Geophysical Research Letters*, *36*(24). https://doi.org/10.1029/2009GL041251

Jiang, X. W., Wang, X. S., Wan, L., & Ge, S. (2011). An analytical study on stagnation points in nested flow systems in basins with depth-decaying hydraulic conductivity. *Water Resources Research*, *47*(1). https://doi.org/10.1029/2010WR009346

Kasahara, T., & Wondzell, S. M. (2003). Geomorphic controls on hyporheic exchange flow in mountain streams. *Water Resources Research*, *39*(1), SBH-3.

Kasahara, T., Datry, T., Mutz, M., & Boulton, A. J. (2009). Treating causes not symptoms: restoration of surface–groundwater interactions in rivers. *Marine and freshwater research*, *60*(9), 976-981.

Käser, D. H., Binley, A., & Heathwaite, A. L. (2013). On the importance of considering channel microforms in groundwater models of hyporheic exchange. *River Research and Applications*, *29*(4), 528-535. https://doi.org/10.1002/rra.1618

Krause, S., Hannah, D. M., Fleckenstein, J. H., Heppell, C. M., Kaeser, D., Pickup, R., ... & Wood, P. J. (2011). Inter-disciplinary perspectives on processes in the hyporheic zone. *Ecohydrology*, *4*(4), 481-499.

Krause, S., & Blume, T. (2013). Impact of seasonal variability and monitoring mode on the adequacy of fiber-optic distributed temperature sensing at aquifer-river interfaces. *Water Resources Research*, *49*(5), 2408-2423.

Landmeyer, J. E., Bradley, P. M., Trego, D. A., Hale, K. G., & Haas, J. E. (2010). MTBE, TBA, and TAME attenuation in diverse hyporheic zones. *Groundwater*, *48*(1), 30-41.

Laudon, H., Sjöblom, V., Buffam, I., Seibert, J., & Mörth, M. (2007). The role of catchment scale and landscape characteristics for runoff generation of boreal streams. *Journal of Hydrology*, *344*(3-4), 198-209.

Laudon, H., Berggren, M., Ågren, A., Buffam, I., Bishop, K., Grabs, T., ... & Köhler, S. (2011). Patterns and dynamics of dissolved organic carbon (DOC) in boreal streams: the role of processes, connectivity, and scaling. *Ecosystems*, *14*(6), 880-893.

Laudon, H., Taberman, I., Ågren, A., Futter, M., Ottosson-Löfvenius, M., & Bishop, K. (2013). The Krycklan Catchment Study—A flagship infrastructure for hydrology, biogeochemistry, and climate research in the boreal landscape. *Water Resources Research*, *49*(10), 7154-7158.

Laudon, H., & Löfvenius, M. O. (2016). Adding snow to the picture-providing complementary winter precipitation data to the Krycklan Catchment Study database. *Hydrological Processes*, *30*(13), 2413-2416.

Leach, J. A., Lidberg, W., Kuglerová, L., Peralta-Tapia, A., Ågren, A., & Laudon, H. (2017). Evaluating topography-based predictions of shallow lateral groundwater discharge zones for a boreal lake-stream system. *Water Resources Research*, *53*(7), 5420-5437. https://doi.org/10.1002/2016WR019804

Lee, C. H., & Farmer, I. W. (1993). *Fluid flow in discontinuous rocks*. Chapman & Hall.

Lewandowski, J., Arnon, S., Banks, E., Batelaan, O., Betterle, A., Broecker, T., ... & Gomez-Velez, J. (2019). Is the hyporheic zone relevant beyond the scientific community?. *Water*, *11*(11), 2230. https://doi.org/10.3390/w11112230

Low, D. J., Hippe, D. J., & Yannacci, D. (2002). *Geohydrology of southeastern Pennsylvania* (No. 4166). US Department of the Interior, US Geological Survey.

Lyon, S. W., Grabs, T., Laudon, H., Bishop, K. H., & Seibert, J. (2011). Variability of groundwater levels and total organic carbon in the riparian zone of a boreal catchment. *Journal of Geophysical Research: Biogeosciences*, *116*(G1).

Marklund, L., Wörman, A., Geier, J., Simic, E., & Dverstorp, B. (2008). Impact of landscape topography and quaternary overburden on the performance of a geological repository of nuclear waste. *Nuclear technology*, *163*(1), 165-179.

Marklund, L. (2009). *Topographic control of groundwater flow* (Doctoral dissertation, KTH).

Marklund, L., & Wörman, A. (2011). The use of spectral analysis-based exact solutions to characterize topography-controlled groundwater flow. *Hydrogeology Journal*, 19, 1531– 1543, https://dx.doi.org/10.1007/s10040-011-0768-4

Marzadri, A., Tonina, D., McKean, J. A., Tiedemann, M. G., & Benjankar, R. M. (2014). Multi-scale streambed topographic and discharge effects on hyporheic exchange at the stream network scale in confined streams. *Journal of Hydrology*, *519*, 1997-2011.

Mamer, E. A., & Lowry, C. S. (2013). Locating and quantifying spatially distributed groundwater/surface water interactions using temperature signals with paired fiber-optic cables. *Water Resources Research*, *49*(11), 7670-7680. https://doi.org/10.1002/2013WR014235

Mathers, K. L., Millett, J., Robertson, A. L., Stubbington, R., & Wood, P. J. (2014). Faunal response to benthic and hyporheic sedimentation varies with direction of vertical hydrological exchange. *Freshwater Biology*, *59*(11), 2278-2289. https://doi.org/10.1111/fwb.12430

McClain, M. E., Boyer, E. W., Dent, C. L., Gergel, S. E., Grimm, N. B., Groffman, P. M., ... & Pinay, G. (2003). Biogeochemical hot spots and hot moments at the interface of terrestrial and aquatic ecosystems. *Ecosystems*, 301-312.

Medina, M. A., Doneker, R. L., Grosso, N., Johns, D. M., Lung, W., Mohsen, M. F. N., ... & Roberts, P. J. (2004). Surface water-ground water interactions and modeling applications: Modeling for Management and Remediation. In *Contaminated Ground Water and Sediment: Modeling for Management and Remediation* (pp. 1-62). CRC Press.

Morén, I., Wörman, A., & Riml, J. (2017). Design of remediation actions for nutrient mitigation in the hyporheic zone. *Water Resources Research*, *53*(11), 8872-8899. https://doi.org/10.1002/2016WR020127

National Research Council. (2002). *Riparian areas: functions and strategies for management*. National Academies Press.

Neretnieks, I. (1979). Analysis of some tracer runs in granite rock using a fissure model. In *Scientific Basis for Nuclear Waste Management* (pp. 411-415). Springer, Boston, MA.

Nikora, V. I., Sukhodolov, A. N., & Rowinski, P. M. (1997). Statistical sand wave dynamics in one-directional water flows. *Journal of Fluid Mechanics*, *351*, 17-39.

Nogaro, G., Datry, T., Mermillod-Blondin, F., Foulquier, A., & Montuelle, B. (2013). Influence of hyporheic zone characteristics on the structure and activity of microbial assemblages. *Freshwater Biology*, *58*(12), 2567-2583.

Orghidan, T. (1959). Ein neuer Lebensraum des unterirdischen Wassers: der hyporheische Biotop. *Arch. Hydrobiol*, *55*(3), 392-414.

Peck, M. F., & Payne, D. F. (2003). Development of an estimated water-table map for coastal Georgia and adjacent parts of Florida and South Carolina. Georgia Institute of Technology.

Poole, G. C., Stanford, J. A., Running, S. W., & Frissell, C. A. (2006). Multiscale geomorphic drivers of groundwater flow paths: subsurface hydrologic dynamics and hyporheic habitat diversity. *Journal of the North American Benthological Society*, *25*(2), 288-303. https://doi.org/10.1899/08873593(2006)25[288:MGDOGF]2.0.CO;2

Rau, G. C., Andersen, M. S., McCallum, A. M., & Acworth, R. I. (2010). Analytical methods that use natural heat as a tracer to quantify surface water–groundwater exchange, evaluated using field temperature records. *Hydrogeology Journal*, *18*(5), 1093-1110.

Rinderer, M., Van Meerveld, H. J., & Seibert, J. (2014). Topographic controls on shallow groundwater levels in a steep, prealpine catchment: When are the TWI assumptions valid?. *Water Resources Research*, *50*(7), 6067-6080.

Rodríguez-Iturbe, I., & Rinaldo, A. (1997). *Fractal river basins: chance and self-organization*. Cambridge University Press.

Saar, M. O., & Manga, M. (2004). Depth dependence of permeability in the Oregon Cascades inferred from hydrogeologic, thermal, seismic, and magmatic modeling constraints. *Journal of Geophysical Research: Solid Earth*, *109*(B4).

Salehin, M., Packman, A. I., & Paradis, M. (2004). Hyporheic exchange with heterogeneous streambeds: Laboratory experiments and modeling. *Water Resources Research*, *40*(11).

Sanford, W. (2002). Recharge and groundwater models: an overview. *Hydrogeology journal*, *10*(1), 110-120.

Sawyer, A. H., & Cardenas, M. B. (2009). Hyporheic flow and residence time distributions in heterogeneous cross-bedded sediment. *Water Resources Research*, *45*(8). https://doi.org/10.1029/2008WR007632

Schornberg, C., Schmidt, C., Kalbus, E., & Fleckenstein, J. H. (2010). Simulating the effects of geologic heterogeneity and transient boundary conditions on streambed temperatures—Implications for temperature-based water flux calculations. *Advances in Water Resources*, *33*(11), 1309-1319.

Shaman, J., Stieglitz, M., Engel, V., Koster, R., & Stark, C. (2002). Representation of subsurface storm flow and a more responsive water table in a TOPMODEL-based hydrology model. *Water Resources Research*, *38*(8), 31-1.

Shanafield, M., Hatch, C., & Pohll, G. (2011). Uncertainty in thermal time series analysis estimates of streambed water flux. *Water Resources Research*, *47*(3).

Sharma, S. K., Gajbhiye, S., & Tignath, S. (2015). Application of principal component analysis in grouping geomorphic parameters of a watershed for hydrological modeling. *Applied Water Science*, *5*(1), 89-96.

SKB (2004) RD&D-Programme 2004. Programme for research, development and demonstration of methods for the management and disposal of nuclear waste, including social science research. Swedish Nuclear Fuel and Waste Management Company (SKB), SKB Report TR-04-21.

Singh, T., Wu, L., Gomez-Velez, J. D., Lewandowski, J., Hannah, D. M., & Krause, S. (2019). Dynamic Hyporheic Zones: Exploring the Role of Peak Flow Events on Bedform-Induced Hyporheic Exchange. *Water Resources Research*, *55*(1), 218-235. https://doi.org/10.1029/2018WR022993

Sridhar, H. (2020). The Impact of Boundary Condition on Groundwater Flow: Topography v/s Recharge Controlled.

Stanford, J. A., & Ward, J. V. (1988). The hyporheic habitat of river ecosystems. *Nature*, *335*(6185), 64-66.

Stanford, J. A., & Ward, J. V. (1993). An ecosystem perspective of alluvial rivers: connectivity and the hyporheic corridor. *Journal of the North American Benthological Society*, *12*(1), 48-60.

Streltsova, T. D. (1987). Well testing in heterogeneous formations.

Sterte, E. J., Johansson, E., Sjöberg, Y., Karlsen, R. H., & Laudon, H. (2018). Groundwater-surface water interactions across scales in a boreal landscape investigated using a numerical modelling approach. *Journal of Hydrology*, *560*, 184-201. https://doi.org/10.1016/j.jhydrol.2018.03.011

Stonedahl, S. H., Harvey, J. W., Wörman, A., Salehin, M., & Packman, A. I. (2010), A multiscale model for integrating hyporheic exchange from ripples to meanders. *Water Resources Research*, 46, W12539, https://dx.doi.org/10.1029/2009WR008865.

Tetzlaff, D., Seibert, J., & Soulsby, C. (2009). Inter-catchment comparison to assess the influence of topography and soils on catchment transit times in a geomorphic province; the Cairngorm mountains, Scotland. *Hydrological Processes: An International Journal*, *23*(13), 1874-1886.

Thackston, E. L. (1967). Longitudinal mixing and reaeration in natural streams.

Thackston, E. L., & Schnelle Jr, K. B. (1970). Predicting effects of dead zones on stream mixing. *Journal of the Sanitary Engineering Division*, *96*(2), 319-331.

Tonina, D., & Buffington, J. M. (2007). Hyporheic exchange in gravel bed rivers with pool-riffle morphology: Laboratory experiments and three-dimensional modeling. *Water Resources Research*, *43*(1). https://doi.org/10.1029/2005WR004328

Toth, J. (1963). A theoretical analysis of groundwater flow in small drainage basins. *Journal of geophysical research*, *68*(16), 4795-4812.

Tóth, J. (1970). A conceptual model of the groundwater regime and the hydrogeologic environment. *Journal of Hydrology*, *10*(2), 164-176. https://doi.org/10.1016/0022-1694(70)90186-1

Torudd, J., & Saetre, P. (2013). Assessment of long-term radiological effects on plants and animals from a deep geological repository: No discernible impact detected. *Ambio*, *42*(4), 506-516. https://doi.org/10.1007/s13280-013-0403-9.

Trauth, N., Schmidt, C., Vieweg, M., Maier, U., & Fleckenstein, J. H. (2014). Hyporheic transport and biogeochemical reactions in pool-riffle systems under varying ambient groundwater flow conditions. *Journal of Geophysical Research: Biogeosciences*, *119*(5), 910-928.

Trauth, N., & Fleckenstein, J. H. (2017). Single discharge events increase reactive efficiency of the hyporheic zone. *Water Resources Research*, *53*(1), 779-798.

Turcotte, D. L. (1997). Fractals and chaos in geology and geophysics Cambridge University. *Press, New York*.

Vervier, P. (1990). Surface water-ground water ecotones. *The ecology and Management of Aquatic-terrestrial Ecotones*, *4*, 199.

Wang, C., Gomez-Velez, J. D., & Wilson, J. L. (2018). The importance of capturing topographic features for modeling groundwater flow and transport in mountainous watersheds. *Water Resources Research*, *54*(12), 10-313.

Ward, A. S., Gooseff, M. N., & Singha, K. (2013). How does subsurface characterization affect simulations of hyporheic exchange?. *Groundwater*, *51*(1), 14-28.

Williams, A., Bloomfield, J., Griffiths, K., & Butler, A. (2006). Characterising the vertical variations in hydraulic conductivity within the Chalk aquifer. *Journal of Hydrology*, *330*(1-2), 53-62.

Winter, T. C. (1999). Relation of streams, lakes, and wetlands to groundwater flow systems. *Hydrogeology Journal*, *7*(1), 28-45. https://doi.org/10.1007/s100400050178

Wondzell, S. M. (2015). Groundwater–surface-water interactions: perspectives on the development of the science over the last 20 years. *Freshwater Science*, *34*(1), 368-376.

Wörman, A., Dverstorp, B. A., Klos, R. A., & Xu, S. (2004). Role of the bio-and geosphere interface on migration pathways for 135Cs and ecological effects. *Nuclear technology*, *148*(2), 194-204.

Wörman, A., Packman, A. I., Marklund, L., Harvey, J. W., & Stone, S. H. (2006). Exact three-dimensional spectral solution to surface-groundwater interactions with arbitrary surface topography. *Geophysical research letters*, *33*(7).

Wörman, A., Packman, A. I., Marklund, L., Harvey, J. W., & Stone, S. H. (2007). Fractal topography and subsurface water flows from fluvial bedforms to the continental shield. *Geophysical Research Letters*, *34*(7). https://doi.org/10.1029/2007GL029426

Wu, L., Singh, T., Gomez-Velez, J., Nützmann, G., Wörman, A., Krause, S., & Lewandowski, J. (2018). Impact of dynamically changing discharge on hyporheic exchange processes under gaining and losing groundwater conditions. *Water Resources Research*, *54*(12), 10-076.

Xu, S., Wörman, A., Dverstorp, B., Klos, R., Shaw, G., & Marklund, L. (2008). SSI's independent consequence calculations in support of the regulatory review of the SR-Can safety assessment. *SSI report*, *2008*, 08.

Zarnetske, J. P., Haggerty, R., Wondzell, S. M., & Baker, M. A. (2011). Dynamics of nitrate production and removal as a function of residence time in the hyporheic zone. *Journal of Geophysical Research: Biogeosciences*, *116*(G1).

Zijl, W. (1999). Scale aspects of groundwater flow and transport systems. *Hydrogeology Journal*, *7*(1), 139-150.